Aerospace Science and Technology 91 (2019) 640–655

Contents lists available at ScienceDirect

Aerospace Science and Technology

www.elsevier.com/locate/aescte

Safe multi-cluster UAV continuum deformation coordination

Hossein Rastgoftar *, Ella M. Atkins

Aerospace Engineering Department, University of Michigan, Ann Arbor, MI, USA

ARTICLE INFO

Article history:
Received 29 March 2019
Received in revised form 2 May 2019
Accepted 2 May 2019
Available online 10 May 2019

ABSTRACT

This paper proposes a paradigm for coordination of multiple unmanned aerial vehicle (UAV) clusters in a shared motion space. UAVs are arranged in a finite number of teams each bounded by a leading triangle. Collective motion of each UAV cluster is managed by a continuum deformation defined by three leaders at the vertices of a leading triangle and followers contained within this triangle. Each triangular cluster can deform substantially to support maneuverability in constrained spaces. This paper specifies necessary conditions to guarantee obstacle avoidance as well as collision avoidance within and across all clusters operating in a shared motion space. Given initial and target configurations, an existing planner (A^*) identifies the shortest coordinated leader UAV paths from initial to final configuration in a manner that satisfies safety constraints. An illustrative simulation case study is presented. Continuum deformation containment offers scalability in collision-free UAV motion planning not previously realized in the detect-and-avoid literature. The proposed multi-cluster coordination protocol also extends previous cooperative control to address detect-and-avoid (DAA) given multiple cooperative teams with different destinations.

1. Introduction

Multi-agent system coordination is an active research area. Formation and cooperative control in a multi-agent system can enhance resilience to failure [1], improve efficiency, and reduce mission cost [2]. Applications include surveillance [3], air traffic management [4], formation flight [5–7], and connected vehicle control [8], and cooperative payload transport [9,10]. This paper studies optimal coordination of many UAVs, clustered into distinct teams, flying in a shared airspace. The paper treats agent optimal coordination as a multi-cluster continuum deformation problem and manages team path planning complexity by abstracting each team to a triangular geometry defined by three leaders.

1.1. Related work

Virtual structure, consensus, containment control, and continuum deformation are available methods for agent coordination in a $3D$ motion space. A virtual structure centrally coordinates agents; each agent's desired position is defined by a reference position vector and a relative displacement vector with respect to this reference [11]. If the agents' relative distances from the reference position remain constant, the multi-agent system can be treated as a rigid body [12]. A flexible virtual structure formation control has also been proposed [13].

Consensus [14–16], containment [17,18], and continuum deformation [19–23] are decentralized multi-agent system (MAS) coordination approaches. Consensus is the most common approach for MAS formation and cooperative control. Both leaderless [14] and leader-based consensus [16,24] approaches have been proposed. Consensus coordination under switching and fixed communication topologies is studied in Refs. [25–27]. Stability of consensus in the presence of communication delays is analyzed in Refs. [28,29]. Finite time consensus control of multi-agent systems is studied in Refs. [30,31].

Similar to consensus, containment control is a decentralized coordination approach. Under containment control, leaders move independently and guide overall team motion. Follower agents communicate with in-neighbor agents to coordinate motions through local communication [17,18]. Containment control under fixed and switching communication topologies is studied in [32]. MAS containment control, guided by stationary and moving leaders, is studied in [33]. Retarded containment control stability is analyzed in [34]. Finite-time MAS containment control [35] and containment control of heterogeneous MAS [36] have also been studied.

Continuum deformation is inspired by the principles of continuum mechanics. Under continuum deformation, inter-agent distance can change over time while inter-agent collision avoidance can be guaranteed [37,38]. Leader-follower formation control via continuum deformation was developed in [21]. Ref. [21] formulates an n-dimensional $(n = 1, 2, 3)$ homogeneous transformation based

* Corresponding author.
E-mail addresses: hosseinr@umich.edu (H. Rastgoftar), ematkins@umich.edu (E.M. Atkins).

https://doi.org/10.1016/j.ast.2019.05.002
1270-9638/

on trajectories of $n+1$ leaders forming an n-dimensional polytope in a $3D$ motion space. Ref. [21] shows how follower agents can acquire desired trajectories through local communication. Decentralized continuum deformation coordination using area preservation and alignment strategy are demonstrated in [20] and [23]; Ref. [19] analyzes stability of continuum deformation coordination in the presence of communication delay. Sufficient conditions for inter-agent collision avoidance are defined in [19,20] while [22] formulates continuum deformation coordination under switching communication topologies.

Robot and vehicle motion planning has been widely studied. Optimal graph search planning methods include dynamic programming [39] which given an admissible heuristic can improve search-space ordering in A* [40]. Rapidly-expanding Random Trees (RRT) [41] were proposed to offer a real-time graph search method applicable for path planning in known and unknown environments. Model predictive control (MPC) [42] is a well-known approach for trajectory (control vector) optimization that accounts for motion costs and vehicle dynamics constraints [43]. Researchers have proposed centralized [44–46] and decentralized [47–49] approaches for multi-agent path planning. Ref. [44] applies A* for first responder multi-agent team planning in a cluttered environment while Ref. [45] applies mixed integer programming. Multi-agent path planning using decentralized RRT is studied in Ref. [48]. Decentralized coordination of mini drones is investigated in Ref. [49]. Furthermore, Ref. [50] proposes a digital pheromones approach for autonomous coordination of a UAV team.

1.2. Contribution and outlines

This paper extends our previous contributions in single-cluster continuum deformation to support multi-cluster continuum deformation coordination over many UAVs. To manage coordination computational complexity, UAVs are clustered into multiple teams, where each team or cluster forms a bounded triangular geometry that evolves internally as particles of a deformable body or continuum. Given initial and target configurations for each UAV cluster, optimal team leader paths are planned to meet waypoint objectives and satisfy safety constraints. A feedback linearization controller performs optimal trajectory tracking. Compared to related work, this paper offers the following contributions:

- An innovative hierarchical coordination strategy is proposed to manage computational and coordination complexity. At the top level cluster leader UAV trajectories are optimized and deconflicted. The remaining follower UAVs are contained within their cluster's leading triangle thus pose no collision risk to other teams. Centralized (top-level) and decentralized (cluster-level) approaches are combined to optimize multi-cluster continuum deformation in a shared motion space. Collective motion of many UAVs, clustered into a finite number of groups, can be optimized with modest computation cost.
- Formal mathematical analysis assures UAV cluster containment and privacy. Cluster containment assures no UAV leaves the cluster over the entire collective motion period. Cluster privacy guarantees that a cluster is not trespassed (entered) by any agent from another cluster over the entire collective motion period. Continuum deformation is applied to assure inter-agent collision avoidance for any two agents within the same cluster.
- To the best of our knowledge, this is the first paper studying collective motion optimization of deformable clusters in a shared motion space. Cluster deformability enables flight through narrow passages and in constrained airspace volumes while allowing the cluster to resume an optimal geometric configuration for flight through open airspace. The paper formally verifies safety and mathematically formulates inter-agent collision avoidance conditions.

The paper is organized as follows. Preliminaries on graph theory, coordinate systems, and continuum deformation are presented in Section 2. Cluster containment and privacy are mathematically formulated in Section 3. The multi-cluster optimization problem is defined in Section 4, followed by formulation of a path-planning optimization strategy in Section 5. UAV dynamics and control are presented in Sections 6. Simulation case study results in Section 7 are followed by concluding remarks in Section 8.

2. Preliminaries

2.1. Coordinate systems

We define a ground coordinate system with bases $\hat{\mathbf{e}}_1$, $\hat{\mathbf{e}}_2$, $\hat{\mathbf{e}}_3$. Bases of the ground coordinate system are fixed in an inertial reference. Each UAV has its own local or body coordinate system. Bases of the body coordinate system of UAV i are denoted by $\mathbf{i}_{b,i}^j$, $\mathbf{j}_{b,i}^j$, and $\mathbf{k}_{b,i}^j$, where subscript $i\in\mathcal{V}^j$ denotes the quadcopter index number and superscript $j\in\Omega_{CL}$ assigns the cluster index number. Cluster identification numbers are defined by the set $\Omega_{CL}=\{1,\cdots,m\}$. Using a $3-2-1$ Euler angle rotation, $\mathbf{i}_{b,i}^j$, $\mathbf{j}_{b,i}^j$, and $\mathbf{k}_{b,i}^j$ are related to $\hat{\mathbf{e}}_1$, $\hat{\mathbf{e}}_2$, $\hat{\mathbf{e}}_3$ by

$$j\in\Omega_{CL},\ i\in\mathcal{V}^j,\qquad \begin{bmatrix}\hat{\mathbf{i}}_{b,i}^j\\ \hat{\mathbf{j}}_{b,i}^j\\ \hat{\mathbf{k}}_{b,i}^j\end{bmatrix}=\mathbf{R}_{\phi_i\theta_i\psi_i}^j\begin{bmatrix}\hat{\mathbf{e}}_1\\ \hat{\mathbf{e}}_2\\ \hat{\mathbf{e}}_3\end{bmatrix} \tag{1a}$$

$$\mathbf{R}_{\phi_i\theta_i\psi_i}^j=\begin{bmatrix}C_{\theta_i^j}C_{\psi_i^j} & C_{\theta_i^j}S_{\psi_i^j} & -S_{\theta_i^j}\\ S_{\phi_i^j}S_{\theta_i^j}C_{\psi_i^j}-C_{\phi_i^j}S_{\psi_i^j} & S_{\phi_i^j}S_{\theta_i^j}S_{\psi}^j+C_{\phi_i^j}C_{\psi_i^j} & S_{\phi_i^j}C_{\theta_i^j}\\ C_{\phi_i^j}S_{\theta_i^j}C_{\psi_i^j}+S_{\phi_i^j}S_{\psi_i^j} & C_{\phi_i^j}S_{\theta_i^j}S_{\psi_i^j}-S_{\phi_i^j}C_{\psi} & C_{\phi_i^j}C_{\theta_i^j}\end{bmatrix}, \tag{1b}$$

where ϕ_i^j, θ_i^j, and ψ_i^j are the roll, pitch, and yaw angles of UAV $i\in\mathcal{V}^j$. Also, $C_{(\cdot)}^j$ and $S_{(\cdot)}^j$ stand for $\cos(\cdot)$ and $\sin(\cdot)$, respectively.

2.2. Position terminology

In this paper, the **actual position** of UAV $i\in\mathcal{V}^j$ is given by

$$j\in\Omega_{CL},\ i\in\mathcal{V}^j,\qquad \mathbf{r}_i^j=x_i^j\hat{\mathbf{e}}_1+y_i^j\hat{\mathbf{e}}_2+z_i^j\hat{\mathbf{e}}_3. \tag{2}$$

The **global desired position** of agent $i\in\mathcal{V}^j$ is denoted by

$$j\in\Omega_{CL},\ i\in\mathcal{V}^j,\qquad \mathbf{r}_{i,HT}^j=x_{i,HT}^j\hat{\mathbf{e}}_1+y_{i,HT}^j\hat{\mathbf{e}}_2+z_{i,HT}^j\hat{\mathbf{e}}_3. \tag{3}$$

In Section 2.4, global desired coordination, treated as continuum deformation, is formulated. This paper assumes that the z components of the global desired positions of all UAVs are the same:

$$\forall j\in\Omega_{CL},\ \forall i\in\mathcal{V}^j,\qquad z_{i,HT}^j=z_{HT}.$$

Local desired position, denoted by $\mathbf{r}_{d,i}^j$ ($i\in\mathcal{V}^j$), is defined:

$$j\in\Omega_{CL},\qquad \mathbf{r}_{d,i}^j=\begin{cases}\mathbf{r}_{i,HT}^j & i\in\mathcal{V}_L^j\\ \sum_{l\in\mathcal{N}_i^j}w_{i,l}^j\mathbf{r}_l^j & i\in\mathcal{V}_F^j\end{cases}, \tag{4}$$

where communication weight $w_{i,l}^j$ is positive and $\sum_{\mathcal{N}_i^j}w_{i,l}^j=1$. In this paper, we assume communication weights are constant and consistent with UAV initial positions. Communication weight characteristic equations are obtained in Section 2.5.

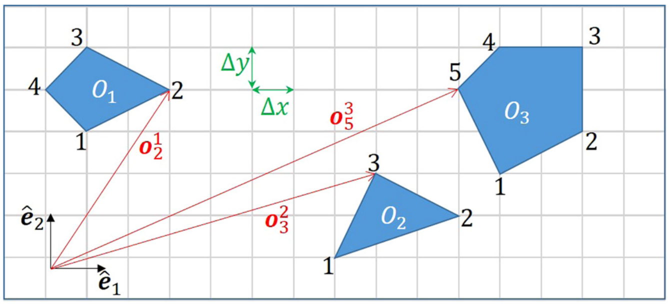

Fig. 1. An example rectangular shared airspace $\mathcal{MO}$ with three obstacles O_1, O_2, and O_3. (For interpretation of the colors in the figure(s), the reader is referred to the web version of this article.)

Initial position of agent $i \in \mathcal{V}^j$ is denoted by

$$j \in \Omega_{CL},\ i \in \mathcal{V}^j, \qquad \mathbf{r}_{i,0}^j = x_{i,0}^j \hat{\mathbf{e}}_1 + y_{i,0}^j \hat{\mathbf{e}}_2 + z_{i,0}^j \hat{\mathbf{e}}_3. \tag{5}$$

Target position of agent $i \in \mathcal{V}^j$ is denoted by

$$j \in \Omega_{CL},\ i \in \mathcal{V}^j, \qquad \mathbf{r}_{i,F}^j = x_{i,F}^j \hat{\mathbf{e}}_1 + y_{i,F}^j \hat{\mathbf{e}}_2 + z_{i,F}^j \hat{\mathbf{e}}_3. \tag{6}$$

2.3. *Definitions of shared airspace, no-flight zones (NFZ), and navigable (NAV) zones*

Let $\mathcal{MO} \subset \mathbb{R}^2$ be a closed set defining a finite two-dimensional *shared airspace*. Let Ω_{NFZ} be a set consisting of n_o convex polygons enclosing obstacles or No-Flight Zones. Mathematically speaking,

$$\Omega_{\text{NFZ}} = \{O_1, \cdots, O_{n_o}\}, \tag{7}$$

where $O_i = O_i\left(\mathbf{o}_1^i, \cdots, \mathbf{o}_{p_i}^i\right) \subset \mathcal{MO}$ $(i = 1, \cdots, n_o)$ denotes the convex polygon $(i = 1, \cdots, n_o)$ defined as follows:

$$i = 1, \cdots, n_o, \qquad O_i = \left\{ \sum_{k=1}^{p_i} \zeta_k^i \mathbf{o}_k^i \middle| \zeta_k^i \geq 0, \sum_{k=1}^{p_i} \zeta_k^i = 1 \right\}, \tag{8}$$

where

$$\mathbf{o}_k^i = o_{k,x}^i \hat{\mathbf{e}}_1 + o_{k,y}^i \hat{\mathbf{e}}_2 \in \mathcal{MO}$$

is the position of the vertex k of convex polygon O_i and $\sum_{k=1}^{p_i} \zeta_k^i \mathbf{o}_k^i$ $(i = 1, \cdots, n_o,\ k = 1, \cdots, p_i,\ \zeta_k^i \geq 0)$ is an interior or boundary point of convex polygon O_i. Navigable Zone

$$\Omega_{\text{NAV}} = \mathcal{MO} \setminus \Omega_{\text{NFZ}} \tag{9}$$

is an open set denoting an obstacle-free or navigable airspace. Notice that $\partial\Omega_{\text{NFZ}}$ defines the boundary of No-Flight Zone Ω_{NFZ}.

Shown in Fig. 1 is the schematic for a shared space containing three obstacles, denoted by O_1, O_2, and O_3. Obstacle O_1 is a quadrilateral $(p_1 = 4)$, obstacle O_2 is a triangle $(p_2 = 3)$, and obstacle O_3 is a pentagon $(p_3 = 5)$.

Motion space discretization: A uniform grid is distributed over the motion space $\mathcal{MO}$. Define distance increments $\Delta x > 0$ and $\Delta y > 0$, grid nodes are mathematically defined by

$$\bar{\mathcal{MO}} = \{(\bar{x}, \bar{y}) \left| \bar{x} = x_0 + k_x \Delta x, \right.$$
$$\bar{y} = y_0 + k_y \Delta y,\ k_x, k_y = 0, 1, 2, \cdots\}.$$

Key Assumption 1. This paper assumes that vertices of the polygons O_1 through O_{n_o} are all positioned at the grid nodes defined by $\bar{\mathcal{MO}}$. Mathematically speaking,

$$\forall i \in \Omega_{\text{NFX}}, k = 1, \cdots, p_i, \qquad \mathbf{o}_k^i \in \bar{\mathcal{MO}}.$$

2.4. *Continuum deformation coordination definition*

Consider a group of N UAVs divided into m clusters. Let

$$j = \Omega_{CL}, \qquad \mathcal{V}^j = \{\mathcal{V}_L^j, \mathcal{V}_F^j\},$$

define local UAV index numbers in cluster $j \in \Omega_{CL}$, where $\mathcal{V}_L^j = \{1, 2, 3\}$ define three leaders and $\mathcal{V}_F^j = \{4, \cdots, N_j\}$ define all followers in cluster j. It is assumed that cluster j contains N_j UAVs $(\sum_{j=1}^m N_j = N)$. Note that each UAV is identified by a cluster number $j \in \Omega_{CL}$ and a local index number $i \in \mathcal{V}^j$. The paper treats UAVs in cluster j as a finite number of particles of a deformable body or continuum.[1] The desired coordination of cluster j is defined by a homogeneous transformation:

$$t \geq t_0,\ j \in \Omega_{CL},\ i \in \mathcal{V}^j, \qquad \mathbf{r}_{i,HT}^j = \mathbf{Q}^j(t, t_0)\mathbf{r}_{i,0}^j + \mathbf{d}^j(t, t_0), \tag{10}$$

where t_0 is the initial time and $\mathbf{Q}^j \in \mathbb{R}^{3\times3}$ and $\mathbf{d}^j \in \mathbb{R}^{3\times1}$ are the continuum deformation Jacobian matrix and rigid body displacement vector, respectively. Without loss of generality, we consider 2-D continuum deformation, where

$$j \in \Omega_{CL}, \qquad \mathbf{Q}^j = \begin{bmatrix} \mathbf{Q}_{\text{CD}}^j & \mathbf{0} \\ \mathbf{0} & 1 \end{bmatrix} = \begin{bmatrix} Q_{1,1}^j & Q_{1,2}^j & 0 \\ Q_{2,1}^j & Q_{2,2}^j & 0 \\ 0 & 0 & 1 \end{bmatrix} \tag{11a}$$

$$j \in \Omega_{CL}, \qquad \mathbf{d}^j = \begin{bmatrix} d_1^j & d_2^j & 0 \end{bmatrix}^T. \tag{11b}$$

Elements of $\mathbf{Q}_{\text{CD}}^j$ $(Q_{1,1}^j, Q_{1,2}^j, Q_{2,1}^j, Q_{2,2}^j)$, d_1^j and d_2^j can be defined based on the global desired positions of the leaders [19]:

$$\begin{bmatrix} Q_{1,1}^j(t) \\ Q_{1,2}^j(t) \\ Q_{2,1}^j(t) \\ Q_{2,2}^j(t) \\ d_1^j(t) \\ d_2^j(t) \end{bmatrix} = \begin{bmatrix} x_{1,0}^j & y_{1,0}^j & 0 & 0 & 1 & 0 \\ x_{2,0}^j & y_{2,0}^j & 0 & 0 & 1 & 0 \\ x_{3,0}^j & y_{3,0}^j & 0 & 0 & 1 & 0 \\ 0 & 0 & x_{1,0}^j & y_{1,0}^j & 0 & 1 \\ 0 & 0 & x_{2,0}^j & y_{2,0}^j & 0 & 1 \\ 0 & 0 & x_{3,0}^j & y_{3,0}^j & 0 & 1 \end{bmatrix} \begin{bmatrix} x_{1,HT}^j(t) \\ x_{2,HT}^j(t) \\ x_{3,HT}^j(t) \\ y_{1,HT}^j(t) \\ y_{2,HT}^j(t) \\ y_{3,HT}^j(t) \end{bmatrix}. \tag{12}$$

Polar Decomposition of the Continuum Deformation Jacobian Matrix: Using polar decomposition, $\mathbf{Q}_{\text{CD}}^j$ can be expressed as

$$j \in \Omega_{CL}, \qquad \mathbf{Q}_{\text{CD}}^j = \mathbf{R}_{\text{CD}}^j \mathbf{U}_{\text{CD}}^j, \tag{13}$$

where $\mathbf{U}_{\text{CD}}^j$ is a positive definite (and symmetric) matrix and $\mathbf{R}_{\text{CD}}^j$ is an orthogonal matrix, i.e., $(\mathbf{R}_{\text{CD}}^j)^T \mathbf{R}_{\text{CD}}^j = \mathbf{I}_2$ where $\mathbf{I}_2$ is the identity matrix. Eigenvalues of the matrix $\mathbf{U}_{\text{CD}}^j$ are positive and real and denoted by λ_1^j and λ_2^j $(0 < \lambda_1^j \leq \lambda_2^j)$.

Key Property of a Homogeneous Deformation: Let the three leaders of cluster j form a triangle at all times t. Therefore,

$$\forall t \geq t_0, j \in \Omega_{CL},\ \text{Rank}\left(\begin{bmatrix} \mathbf{r}_{2,HT}^j - \mathbf{r}_{1,HT}^j & \mathbf{r}_{3,HT}^j - \mathbf{r}_{1,HT}^j \end{bmatrix}\right) = 2.$$

The triangle formed by the leaders of cluster $j \in \Omega_{CL}$ is called *leading triangle j*. Under a homogeneous deformation, x and y components of the global desired position of UAV $i \in \mathcal{V}^j$ can be expressed as [19]

[1] A continuum is a continuous domain consisting of infinite number of particles with infinitesimal size [51].

$$j \in \Omega_{CL},\ i \in \mathcal{V}_F^j,\quad \mathcal{Y}_{i,HT}^j = \begin{bmatrix} x_{i,HT}^j(t) \\ y_{i,HT}^j(t) \end{bmatrix} = \sum_{l=1}^{3} \alpha_{i,l}^j \begin{bmatrix} x_{l,HT}^j(t) \\ y_{l,HT}^j(t) \end{bmatrix}, \tag{14}$$

where $\alpha_{i,1}^j$, $\alpha_{i,2}^j$, are $\alpha_{i,3}^j$ **time-invariant** parameters and

$$\alpha_{i,1}^j + \alpha_{i,2}^j + \alpha_{i,3}^j = 1. \tag{15}$$

Parameters $\alpha_{i,1}^j$, $\alpha_{i,2}^j$, are $\alpha_{i,3}^j$ are computed from the initial position of UAV i and the three leaders as follows [19]:

$$j \in \Omega_{CL}, i \in \mathcal{V}_F^j,\qquad \begin{bmatrix} x_{1,0}^j & x_{2,0}^j & x_{3,0}^j \\ y_{1,0}^j & y_{2,0}^j & y_{3,0}^j \\ 1 & 1 & 1 \end{bmatrix} \begin{bmatrix} \alpha_{i,1}^j \\ \alpha_{i,2}^j \\ \alpha_{i,3}^j \end{bmatrix} = \begin{bmatrix} x_{i,0}^j \\ y_{i,0}^j \\ 1 \end{bmatrix}. \tag{16}$$

2.5. Continuum deformation acquisition through local communication

We assume that cluster j's collective motion is guided by three UAV leaders moving independently. Leaders all communicate with each other and evolve in a centralized fashion. However, follower UAVs communicate with local UAVs to update their positions. Inter-agent communication among UAVs is defined by graph $\mathcal{G}^j = \mathcal{G}^j\left(\mathcal{V}^j, \mathcal{E}^j, W^j\right)$, where $\mathcal{E}^j \subset \mathcal{V}^j \times \mathcal{V}^j$ defines edges of the graph $\mathcal{E}^j$. We define

$$j \in \Omega_{CL},\ i \in \mathcal{V}_F^j,\qquad \mathcal{N}_i^j = \left\{ (l,i) \in \mathcal{E}^j \middle| l \in \mathcal{V}^j \right\}$$

as the in-neighbor set of follower UAV $i \in \mathcal{V}_F^j$. Communication of follower $i \in \mathcal{V}_F^j$ with in-neighbor UAV $l \in \mathcal{N}_i^j$ is assigned weights $w_{i,l}^j$, where $\sum_{l\in\mathcal{N}_i^j} w_{i,l}^j = 1$. Communication graph $\mathcal{G}^j$ can be expressed as $\mathcal{G}^j = \partial\Psi^j \cup \Psi^j$, where $\partial\Psi^j \cap \Psi^j = \emptyset$. $\partial\psi^j$ defines the boundary of graph $\mathcal{G}^j$ and sub-graph $\Psi^j = \Psi^j\left(\mathcal{V}_F^j, \mathcal{E}_F^j\right)$ is strongly connected.[2] Ψ^j defines inter-agent communication for followers in cluster $j \in \Omega_{CL}$, i.e., $\mathcal{E}_F^j \subset \mathcal{V}_F^j \times \mathcal{V}_F^j$ defines Ψ^j graph edges. Note that nodes of the boundary graph $\partial\psi^j$ represents cluster j's leaders and nodes of sub-graph ψ^j represent follower UAVs in cluster $j \in \Omega_{CL}$.

FL and FF Communication Matrices: We define weight matrix $\mathbf{W}^j = [W_{il}^j] \in \mathbb{R}^{(N_j-3)\times N_j}$ with the i,l entry specified as follows:

$$W_{il}^j = \begin{cases} w_{i+3,l}^j & (i+3) \in \mathcal{V}_F^j \wedge l \in \mathcal{N}_{i+3}^j \\ -1 & l = i+3 \\ 0 & \text{otherwise.} \end{cases} \tag{17}$$

Partitioning $\mathbf{W}^j$

$$\mathbf{W}^j = \begin{bmatrix} \mathbf{B}^j & \mathbf{A}^j \end{bmatrix} \in \mathbb{R}^{(N_j-3)\times N_j}, \tag{18}$$

where matrices $\mathbf{B}^j \in \mathbb{R}^{(N_j-3)\times 3}$ and $\mathbf{A}^j \in \mathbb{R}^{(N_j-3)\times(N_j-3)}$ are called *Follower-Leader (or FL) communication matrix* and *Follower-Follower (or FF) communication matrix*, respectively. If communication weight $w_{i,l}^j$ $(\forall i \in \mathcal{V}_F^j,\ \forall j)$ is positive, matrix $\mathbf{A}^j$ is Hurwitz [19].

Followers' Communication Weights in a Continuum Deformation Coordination: Followers' communication weights are assigned based on UAV positions at initial time t_0. Let UAV $i \in \mathcal{V}_F^j$, initially positioned at $\mathbf{r}_{i,0}^j = x_{i,0}^j\hat{\mathbf{e}}_1 + y_{i,0}^j\hat{\mathbf{e}}_2 + z_{i,0}^j\hat{\mathbf{e}}_3$, communicate with in-neighbor i_1, i_2, and i_3 $(i_1, i_2, i_3 \in \mathcal{N}_i^j,\ j \in \Omega_{CL})$, initially positioned at $\mathbf{r}_{i_1,0}^j = x_{i_1,0}^j\hat{\mathbf{e}}_1 + y_{i_1,0}^j\hat{\mathbf{e}}_2 + z_{i_1,0}^j\hat{\mathbf{e}}_3$, $\mathbf{r}_{i_2,0}^j = x_{i_2,0}^j\hat{\mathbf{e}}_1 + y_{i_2,0}^j\hat{\mathbf{e}}_2 + z_{i_2,0}^j\hat{\mathbf{e}}_3$, and $\mathbf{r}_{i_3,0}^j = x_{i_3,0}^j\hat{\mathbf{e}}_1 + y_{i_3,0}^j\hat{\mathbf{e}}_2 + z_{i_3,0}^j\hat{\mathbf{e}}_3$. It is further assumed that in-neighbor UAVs i_1, i_2, and i_3 form a triangle at the initial time t_0, therefore,

$$\text{Rank}\begin{bmatrix} \mathbf{r}_{i_2,0}^j - \mathbf{r}_{i_1,0}^j & \mathbf{r}_{i_3,0}^j - \mathbf{r}_{i_1,0}^j \end{bmatrix} = 2, \tag{19}$$

and $\mathbf{r}_{i,0}^j$ is uniquely expressed as follows:

$$\begin{aligned} \mathbf{r}_{i,0}^j &= w_{i,i_2}^j\left(\mathbf{r}_{i_2,0}^j - \mathbf{r}_{i_1,0}^j\right) + w_{i,i_3}^j\left(\mathbf{r}_{i_3,0}^j - \mathbf{r}_{i_1,0}^j\right) \\ &= \left(1 - w_{i,i_2}^j - w_{i,i_3}^j\right)\mathbf{r}_{i_1,0}^j + w_{i,i_2}^j\mathbf{r}_{i_2,0}^j + w_{i,i_3}^j\mathbf{r}_{i_3,0}^j \end{aligned}. \tag{20}$$

Defining $w_{i,1}^j = 1 - w_{i,i_2}^j - w_{i,i_3}^j$, communication weights w_{i,i_1}^j, w_{i,i_2}^j, and w_{i,i_3}^j are uniquely obtained by

$$\begin{bmatrix} x_{i_1,0}^j & x_{i_2,0}^j & x_{i_3,0}^j \\ y_{i_1,0}^j & y_{i_2,0}^j & y_{i_3,0}^j \\ 1 & 1 & 1 \end{bmatrix} \begin{bmatrix} w_{i,i_1}^j \\ w_{i,i_2}^j \\ w_{i,i_3}^j \end{bmatrix} = \begin{bmatrix} x_{i,0}^j \\ y_{i,0}^j \\ 1 \end{bmatrix}. \tag{21}$$

If follower $i \in \mathcal{V}_F^j$ is inside the communication triangle defined by $i_1, i_2, i_3 \in \mathcal{N}_i^j$, then communication weights are all positive [19].

Proposition 1. *Define*

$$\mathcal{Z}_{X,L,0}^j = \begin{bmatrix} x_{1,0}^j & x_{2,0}^j & x_{3,0}^j \end{bmatrix}^T, \tag{22a}$$

$$\mathcal{Z}_{Y,L,0}^j = \begin{bmatrix} y_{1,0}^j & y_{2,0}^j & y_{3,0}^j \end{bmatrix}^T, \tag{22b}$$

$$\mathcal{Z}_{X,F,0}^j = \begin{bmatrix} x_{4,0}^j & \cdots & x_{M^j,0}^j \end{bmatrix}^T, \tag{22c}$$

$$\mathcal{Z}_{Y,F,0}^j = \begin{bmatrix} y_{4,0}^j & \cdots & y_{M^j,0}^j \end{bmatrix}^T. \tag{22d}$$

If communication weights satisfy Eq. (21), then the x and y components of cluster j's UAVs satisfy the following relations [19]:

$$\mathbf{B}^j\mathcal{Z}_{X,L,0}^j + \mathbf{A}^j\mathcal{Z}_{X,F,0}^j = \mathbf{0}, \tag{23a}$$

$$\mathbf{B}^j\mathcal{Z}_{Y,L,0}^j + \mathbf{A}^j\mathcal{Z}_{Y,F,0}^j = \mathbf{0}, \tag{23b}$$

where $\mathbf{A}^j$ and $\mathbf{B}^j$ are determined from Eqs. (17) and (18).

Proposition 2. *If followers' communication weights are consistent with agents' initial positions and satisfy Eq. (21), then the FL communication matrix $\mathbf{B}^j \in \mathbb{R}^{(N_j-3)\times 3}$ and the FF communication matrix $\mathbf{A}^j \in \mathbb{R}^{(N_j-3)\times(N_j-3)}$, obtained by Eqs. (17) and (18), satisfy the following relation [19]:*

$$\mathbf{W}_L^j = \mathbf{A}^{j^{-1}}\mathbf{B}^j = \begin{bmatrix} \alpha_{4,1}^j & \alpha_{4,2}^j & \alpha_{4,3}^j \\ \vdots & \vdots & \vdots \\ \alpha_{N_j,1}^j & \alpha_{N_j,2}^j & \alpha_{N_j,3}^j \end{bmatrix}, \tag{24}$$

where $\alpha_{i,l}^j$ is uniquely assigned using Eq. (16) given initial position of follower $i \in \mathcal{V}_F^j$ and leaders of cluster j.

UAV Global Desired Trajectories: Defining $\mathcal{Z}_{q,L,HT}^j(t) = [q_{1,HT}^j(t)\quad q_{2,HT}^j(t)\quad q_{3,HT}^j(t)]^T$ and $\mathcal{Z}_{q,F,HT}^j(t) = [q_{4,HT}^j(t)\cdots q_{N_j,HT}^j(t)]^T$ $(q = x, y)$, components of the global desired trajectories are defined by

$$j \in \Omega_{CL},\ q = x, y,\ \forall t,\qquad \mathcal{Z}_{q,F,HT}^j(t) = \mathbf{W}_L^j\mathcal{Z}_{q,L,HT}^j(t). \tag{25}$$

[2] Directed graph $\mathcal{G}^j = \mathcal{G}^j\left(\mathcal{V}^j, \mathcal{E}^j\right)$, is called *strongly collected*, if there are directed paths from $i \in \mathcal{V}^j$ to $l \in \mathcal{V}^j$ and l to i $(\forall i, l \in \mathcal{V}^j,\ i \neq l)$.

3. Safety requirements: obstacle collision avoidance cluster containment and cluster privacy

Before proceeding to specify continuum deformation safety requirements, we define

$$\begin{bmatrix} a_1^j \\ a_2^j \\ a_3^j \end{bmatrix} = \begin{bmatrix} x_{1,HT}^j & x_{2,HT}^j & x_{3,HT}^j \\ y_{1,HT}^j & y_{2,HT}^j & y_{3,HT}^j \\ 1 & 1 & 1 \end{bmatrix}^{-1} \begin{bmatrix} x \\ y \\ 1 \end{bmatrix},$$

where $a_h^j = a_h^j\left(x_{1,HT}^j, x_{2,HT}^j, x_{3,HT}^j, x, y_{1,HT}^j, y_{2,HT}^j, y_{3,HT}^j, y\right)$ $(h \in \mathcal{V}_L)$, $\mathbf{r} = x\hat{\mathbf{e}}_1 + y\hat{\mathbf{e}}_2$ is the position of a point in the $x-y$ plane and $x_{l,HT}^j$ and $y_{l,HT}^j$ are position components of leader $l \in \mathcal{V}_L^j$. The solution of Eq. (16) can be expressed as

$$a_r^j = \frac{(x_{q,HT}^j - x_{p,HT}^j)(y - y_{p,HT}^j) - (y_{q,HT}^j - y_{p,HT}^j)(x - x_{p,HT}^j)}{(x_{q,HT}^j - x_{p,HT}^j)(y_{r,HT}^j - y_{p,HT}^j) - (y_{r,HT}^j - y_{p,Ht}^j)(x_{r,HT}^j - x_{p,HT}^j)}, \tag{26}$$

where

$$(p, q, r) \in \left\{(1,2,3), (2,3,1), (3,1,2)\right\}. \tag{27}$$

Both cluster containment and privacy must be satisfied and obstacle collision avoidance must be ensured in a safe multi-cluster continuum deformation. Propositions 3, 4, and 5 formulate these three necessary conditions. By ensuring cluster containment, follower quadopter of cluster $j \in \Omega_{CL}$ does not leave the cluster at any time t. By ensuring cluster privacy, a cluster is not trespassed by a UAV from a different cluster. Proposition 5 provides gaurantee condition for obstacle collision avoidance.

Key Assumption 2. In this paper, we assume that the desired waypoint of leader i, denoted by $\left(\bar{x}_{i,HT}^j, \bar{y}_{i,HT}^j\right)$, is positioned on the motion space grid nodes. Mathematically speaking,

$$j \in \Omega_{CL}, i \in \mathcal{V}_L^j, \qquad \left(\bar{x}_{i,HT}^j, \bar{y}_{i,HT}^j\right) \in \bar{\mathcal{MO}}.$$

Proposition 3 *(Containment condition). Followers are all inside the leading triangle $j \in \Omega_{CL}$ at any time t, if*

$$\forall i \in \mathcal{V}_F^j, \qquad \left(a_1^j \geq 0\right) \wedge \left(a_2^j \geq 0\right) \wedge \left(a_3^j \geq 0\right), \tag{28}$$

where $a_r^j = a_r^j\left(x_{1,HT}^j, x_{2,HT}^j, x_{3,HT}^j, x_{i,HT}^j, y_{1,HT}^j, y_{2,HT}^j, y_{3,HT}^j, y_{i,HT}^j\right)$ $(r = 1, 2, 3, \forall i \in \mathcal{V}_F)$.

Proof. $a_r^j = \text{constant}$ $(r = 1, 2, 3)$ is an equation of the line parallel to the line segments connecting leaders p and q $(p \neq q,\ q \neq r,\ r \neq p,\ p, q, r \in \{1, 2, 3\})$. If follower $i \in \mathcal{V}_F^j$ is located along the line segment connecting leaders p and q, the denominator of Eq. (16) vanishes and $a_{i,r}^j = 0$. Considering the signs of parameters a_1^j, a_2^j, and a_3^j $(j \in \Omega_{CL}, i \in \mathcal{V}_F^j)$, the horizontal plane is divided into the following 10 zones:

$$\text{Zone 1}: a_{i,1}^j > 0,\ a_{i,2}^j > 0,\ a_{i,3}^j > 0.$$

$$\text{Zone 2}: a_{i,1}^j > 0,\ a_{i,2}^j > 0,\ a_{i,3}^j < 0.$$

$$\text{Zone 3}: a_{i,1}^j > 0,\ a_{i,2}^j < 0,\ a_{i,3}^j > 0.$$

$$\text{Zone 4}: a_{i,1}^j < 0,\ a_{i,2}^j > 0,\ a_{i,3}^j > 0.$$

$$\text{Zone 5}: a_{i,1}^j < 0,\ a_{i,2}^j < 0,\ a_{i,3}^j > 0.$$

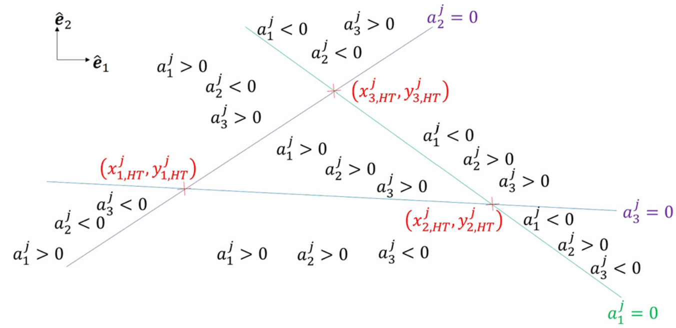

Fig. 2. $x-y$ plane partitioning into 10 zones based on the signs of parameters $a_1^j(x_{i,HT}, y_{i,HT})$, $a_2^j(x_{i,HT}, y_{i,HT})$, and $\alpha_{i,3}^j(x_{i,HT}, y_{i,HT})$ $(j \in \Omega_{CL}, i \in \mathcal{V}_F^j)$.

$$\text{Zone 6}: a_{i,1}^j > 0,\ a_{i,2}^j < 0,\ a_{i,3}^j < 0.$$

$$\text{Zone 7}: a_{i,1}^j < 0,\ a_{i,2}^j > 0,\ a_{i,3}^j < 0.$$

$$\text{Zone 8}: a_{i,i_1} = 0.$$

$$\text{Zone 9}: a_{i,2}^j = 0.$$

$$\text{Zone 10}: a_{i,3}^j = 0.$$

As shown in Fig. 2 $\alpha_{1,2}^j$, $\alpha_{2,3}^j$, and $\alpha_{3,1}^j$ are all positive, only if follower $i \in \mathcal{V}_F^j$ is inside leading triangle $j \in \Omega_{CL}$. □

Proposition 4 *(Privacy condition). It is ensured that cluster $j_1 \in \Omega_{CL}$ is not trespassed by a UAV $i_2 \in \mathcal{V}^{j_2}$ at any time t, if*

$$\begin{aligned} &\forall j_1, j_2 \in \Omega_{CL}, j_1 \neq j_2,\ \forall i_2 \in \mathcal{V}^{j_2} \\ &\left(a_1^{j_1}\left(\bar{x}_{1,HT}^{j_1}, \bar{x}_{2,HT}^{j_1}, \bar{x}_{3,HT}^{j_1}, \bar{x}_{i_2,HT}^{j_2}, \bar{y}_{1,HT}^{j_1}, \bar{y}_{2,HT}^{j_1}, \bar{y}_{3,HT}^{j_1}, \bar{y}_{i_2,HT}^{j_2}\right) < 0\right) \vee \\ &\left(a_2^{j_1}\left(\bar{x}_{1,HT}^{j_1}, \bar{x}_{2,HT}^{j_1}, \bar{x}_{3,HT}^{j_1}, \bar{x}_{i_2,HT}^{j_2}, \bar{y}_{1,HT}^{j_1}, \bar{y}_{2,HT}^{j_1}, \bar{y}_{3,HT}^{j_1}, \bar{y}_{i_2,HT}^{j_2}\right) < 0\right) \vee \\ &\left(a_3^{j_1}\left(\bar{x}_{1,HT}^{j_1}, \bar{x}_{2,HT}^{j_1}, \bar{x}_{3,HT}^{j_1}, \bar{x}_{i_2,HT}^{j_2}, \bar{y}_{1,HT}^{j_1}, \bar{y}_{2,HT}^{j_1}, \bar{y}_{3,HT}^{j_1}, \bar{y}_{i_2,HT}^{j_2}\right) < 0\right). \end{aligned} \tag{29}$$

Proof. If UAV $i_2 \in \mathcal{V}^{j_2}$ is outside cluster j_1, then, $a_1^{j_1}\left(\bar{x}_{1,HT}^{j_1}, \bar{x}_{2,HT}^{j_1}, \bar{x}_{3,HT}^{j_1}, \bar{x}_{i_2,HT}^{j_2}, \bar{y}_{1,HT}^{j_1}, \bar{y}_{2,HT}^{j_1}, \bar{y}_{3,HT}^{j_1}, \bar{y}_{i_2,HT}^{j_2}\right)$, $a_2^{j_1}\left(\bar{x}_{1,HT}^{j_1}, \bar{x}_{2,HT}^{j_1}, \bar{x}_{3,HT}^{j_1}, \bar{x}_{i_2,HT}^{j_2}, \bar{y}_{1,HT}^{j_1}, \bar{y}_{2,HT}^{j_1}, \bar{y}_{3,HT}^{j_1}, \bar{y}_{i_2,HT}^{j_2}\right)$, and $a_3^{j_1}\left(\bar{x}_{1,HT}^{j_1}, \bar{x}_{2,HT}^{j_1}, \bar{x}_{3,HT}^{j_1}, \bar{x}_{i_2,HT}^{j_2}, \bar{y}_{1,HT}^{j_1}, \bar{y}_{2,HT}^{j_1}, \bar{y}_{3,HT}^{j_1}, \bar{y}_{i_2,HT}^{j_2}\right)$ $(j \in \Omega_{CL}, i \in \mathcal{V}_F^j)$ cannot be all non-negative (See Fig. 2). Therefore, privacy of cluster j_1 is assured if condition (29) is satisfied for all UAVs in cluster j_2. □

Proposition 5 *(Obstacle collision avoidance). Cluster $j \in \Omega_{CL}$ is assured to not collide with obstacle $O_i = O_i\left(\mathbf{o}_1^i, \cdots, \mathbf{o}_{p_i}^i\right)$, i.e., cluster j does not enter No-Flight Zone O_i, if*

$$\begin{aligned} &i = 1, \cdots, n_o,\ O_i \in \Omega_{\text{NFZ}},\ \forall j \in \Omega_{CL},\ k = 1, \cdots, p_i \\ &a_1^j\left(\bar{x}_{1,HT}^j, \bar{x}_{2,HT}^j, \bar{x}_{3,HT}^j, o_{k,x}^i, \bar{y}_{1,HT}^j, \bar{y}_{2,HT}^j, \bar{y}_{3,HT}^j, o_{k,y}^i\right) \vee \\ &a_2^j\left(\bar{x}_{1,HT}^j, \bar{x}_{2,HT}^j, \bar{x}_{3,HT}^j, o_{k,x}^i, \bar{y}_{1,HT}^j, \bar{y}_{2,HT}^j, \bar{y}_{3,HT}^j, o_{k,y}^i\right) \vee \\ &a_3^j\left(\bar{x}_{1,HT}^j, \bar{x}_{2,HT}^j, \bar{x}_{3,HT}^j, o_{k,x}^i, \bar{y}_{1,HT}^j, \bar{y}_{2,HT}^j, \bar{y}_{3,HT}^j, o_{k,y}^i\right). \end{aligned} \tag{30}$$

Proof. Because obstacles (No-Flight Zones) are convex regions in the shared airspace, the position of any interior point of O_{j_2} can be expressed as a convex combination of vertices $\mathbf{o}_1^{j_2}, \cdots, \mathbf{o}_{p_{j_2}}^{j_2}$.

Therefore, obstacle O_{j_2} can be represented by its vertices and cluster $j_1 \in \Omega_{CL}$ does not collide with obstacle O_{j_2} if condition (30) is satisfied. □

4. Problem statement and formulation

Consider a collection of m UAV clusters in a shared motion space. Each cluster forms a triangular domain and consists of a large number of small UAVs. Three leaders, located at the vertices of a triangular cluster, guide the collective motion. It is assumed that initial and target configurations of each triangular cluster are known. Given initial and target configurations, the objective is to minimize travel distance (path length) of every UAV from its initial destination to its target location ensuring inter-agent and obstacle collision avoidance, i.e., “No-Flight Zone” avoidance.

This problem is mathematically defined as follows:

$$\min \sum_{j\in\Omega_{CL}} \sum_{i\in\mathcal{V}^j} \int_0^{S^j_{i,f}} \mathrm{d}S, \tag{31}$$

subject to containment, privacy, and obstacle avoidance guarantee conditions (28), (29), and (30) as well as the following constraints:

$$\forall j_1, j_2 \in \Omega_{CL},\ \forall i \in \mathcal{V}^{j_1}, \forall l \in \mathcal{V}^{j_2},\ i \neq l,\quad \|\mathbf{r}_i^{j_1} - \mathbf{r}_l^{j_2}\| > 2\epsilon, \tag{32a}$$

$$j \in \Omega_{CL},\ i \in \mathcal{V}^j, \qquad \mathbf{r}_i^j(0) = \mathbf{r}_{i,0}^j, \tag{32b}$$

$$j \in \Omega_{CL},\ i \in \mathcal{V}^j, \qquad \mathbf{r}_i^j\left(S^j_{i,f}\right) = \mathbf{r}_{i,F}^j, \tag{32c}$$

$$j \in \Omega_{CL}, \qquad \mathrm{Rank}\left(\left[\mathbf{r}^j_{2,HT} - \mathbf{r}^j_{1,HT} \quad \mathbf{r}^j_{3,HT} - \mathbf{r}^j_{1,HT}\right]\right) = 2, \tag{32d}$$

where $\epsilon > 0$ is the radius of a ball enclosing each UAV, and $S^j_{i,f}$ is length of the path connecting initial position $\mathbf{r}^j_{i,0}$ to target position $\mathbf{r}^j_{i,F}$.

Constraint equation (32a) ensures that no two separate UAVs collide. **Constraint equation** (32c) ensures that UAV $i \in \mathcal{V}^j$ ultimately reaches the target destination given the initial position assigned in **constraint equation** (32b). **Constraint equation** (32d) guarantees leaders form a triangle at any time t. Eq. (32d) must be satisfied to ensure that the Jacobian matrix $\mathbf{Q}^j$ is nonsingular at any time t, i.e., if rank condition (32d) is not satisfied, the leading triangle j is either mapped to a line or a single point.

The above optimization problem is highly nonlinear and computationally expensive. To deal with complexity, we assume that each UAV $i \in \mathcal{V}^j$ moves on a straight path over $t \in [t_{k-1}, t_k]$ ($k = 1, 2, \cdots$). Therefore, path planning can be treated as waypoint planning where leaders' paths can be simply planned by connecting consecutive optimal waypoints. The paper applies a well-established A* method to find optimal leader waypoints and optimize continuum deformation of UAV clusters in a shared motion space such that geometric motion constraints are all satisfied. While A* has substantially overhead, its application to only leaders can provide manage complexity sufficiently given a limited number of interacting clusters. Once waypoints are defined, each UAV desired speed profile is then planned along the optimal waypoint sequence as described in Section 5.3.

5. Multi-cluster continuum deformation planning

In this paper we assume that the $x - y$ plane is uniformly discretized. Let

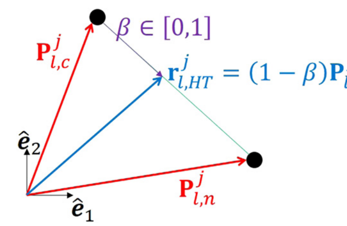

Fig. 3. Straight path of leader $l \in \mathcal{V}_L^j$ between current waypoint $\mathbf{P}^j_{l,c}$ and $\mathbf{P}^j_{l,n}$.

$$j \in \Omega_{CL},\ l = 1, 2, 3, \qquad \mathbf{P}^j_{l,c} = p^j_{x,l,c}\hat{\mathbf{e}}_1 + p^j_{y,l,c}\hat{\mathbf{e}}_2 \in \bar{\mathcal{MO}}$$

define the <u>current</u> desired waypoint of leader $l \in \mathcal{V}^j$. The <u>next</u> waypoint of each leader l is denoted by

$$j \in \Omega_{CL},\ l = 1, 2, 3, \qquad \mathbf{P}^j_{l,n} = p^j_{x,l,n}\hat{\mathbf{e}}_1 + p^j_{y,l,n}\hat{\mathbf{e}}_2 \in \bar{\mathcal{MO}},$$

where

$$q = x, y, \qquad p^j_{q,l,n} = p^j_{q,l,c} + h_q\Delta q \tag{33a}$$

$$q = x, y, \qquad h_q \in \{-1, 0, 1\}. \tag{33b}$$

Note that $\Delta q > 0$ ($q = x, y$) is constant. Let $\bar{\mathbf{T}}^j_c = (\mathbf{P}^j_{1,c}, \mathbf{P}^j_{2,c}, \mathbf{P}^j_{3,c})$ denote the desired configuration of leading triangle $j \in \Omega_{CL}$ ($j \in \{1, \cdots, m\}$) in the $x - y$ plane at the current time. The next desired configuration of leading triangle j is denoted by $\bar{\mathbf{T}}^j_n = (\mathbf{P}^j_{1,n}, \mathbf{P}^j_{2,n}, \mathbf{P}^j_{3,n})$. In addition, $\bar{\mathbf{T}}^j_g = (\mathbf{P}^j_{1,g}, \mathbf{P}^j_{2,g}, \mathbf{P}^j_{3,g})$ and $\bar{\mathbf{T}}^j_0 = (\mathbf{P}^j_{1,0}, \mathbf{P}^j_{2,0}, \mathbf{P}^j_{3,0})$ are the goal and initial configurations of leading triangle $j \in \Omega_{CL}$, where

$$l = 1, 2, 3, \qquad \mathbf{P}^j_{l,g} = p^j_{x,l,g}\hat{\mathbf{e}}_1 + p^j_{y,l,g}\hat{\mathbf{e}}_2 \in \bar{\mathcal{MO}}$$
$$l = 1, 2, 3, \qquad \mathbf{P}^j_{l,0} = p^j_{x,l,0}\hat{\mathbf{e}}_1 + p^j_{y,l,0}\hat{\mathbf{e}}_2 \in \bar{\mathcal{MO}}.$$

We assume leader $l \in \mathcal{V}_L^j$ moves along the line segment connecting $\mathbf{P}^j_{l,c}$ and $\mathbf{P}^j_{l,n}$ (see Fig. 3). The desired path of leader $l \in \mathcal{V}_L^j$ is defined by

$$l \in \mathcal{V}_L^j, \qquad \mathbf{r}^j_{l,HT} = (1-\beta)\mathbf{P}^j_{l,c} + \beta\mathbf{P}^j_{l,n} + z_{HT}\hat{\mathbf{e}}_3, \tag{34}$$

where multi-UAV system (MUS) elevation z_{HT} is constant, $l \in \mathcal{V}_L^j$, $j \in \Omega_{CL}$, and $\beta \in [0, 1]$.

5.1. Collision avoidance

It is computationally expensive to directly check for inter-agent collision avoidance with constraint Eq. (32a) for every UAV pair in the shared motion space. Because each cluster evolution is treated as continuum deformation, inter-agent collision avoidance can be assured with reduced computation cost. For this purpose, we first specify inter-agent collision avoidance and containment guarantee conditions in Theorem 1. Assuming containment guarantee and collision avoidance at every cluster, Theorem 2 provides sufficient conditions for inter-agent collision avoidance between any two agents in the shared motion space.

Theorem 1. *Let d^j_s be the minimum separation distance between two UAVs in cluster $j \in \Omega_{CL}$ at initial time t_0, d^j_b be the minimum distance of a UAV from the edges of the leading triangle $j \in \{1, \cdots, m\}$ at time t_0 (see Fig. 4), and each UAV be enclosed by a ball with radius ϵ. Define*

$$\delta^j_{max} = \min\left\{\frac{1}{2}\left(d^j_s - 2\epsilon\right), \left(d^j_b - \epsilon\right)\right\}. \tag{35}$$

Let $\mathbf{r}^j_{i,HT}$ be the global desired position of a UAV $i \in \mathcal{V}^j$, given by a continuum deformation (see Eq. (10)), $\mathbf{r}^j_i$ be the actual position of UAV $i \in \mathcal{V}^j$,

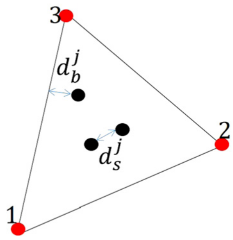

Fig. 4. Schematic of initial leading triangle configuration $j \in \Omega_{CL}$ showing two UAVs having minimum separation distance d_s^j and a UAV with minimum distance d_b^j.

and δ^j be an upper limit for deviation of a cluster j UAV from continuum deformation desired position:

$$\forall t \in [t_k, t_{k+1}],\ \forall i \in \mathcal{V}^j, \qquad \|\mathbf{r}_i^j(t) - \mathbf{r}_{i,HT}^j(t)\| \le \delta^j. \tag{36}$$

Define

$$\lambda_{\text{CD,min}}^j = \frac{\delta^j + \epsilon}{\delta_{max}^j + \epsilon}. \tag{37}$$

If

$$\forall t \in [t_k, t_{k+1}], \qquad \mathcal{C}_{Col,k}^j = \lambda_{\text{CD,min}}^j - \lambda_1^j \left(\mathbf{U}_{\text{CD}}^j(t)\right) \le 0, \tag{38}$$

then,

1. *Inter-agent collision avoidance in cluster j (constraint Eq. (32d)) is guaranteed and*
2. *All followers remain inside leading triangle j at all times t, i.e., containment condition (28) is satisfied.*

Proof. See the proof in [19,20]. □

Theorem 2. *Assume $\mathcal{C}_{col,k}^{j_1}$ and $\mathcal{C}_{col,k}^{j_2}$ ($j_1, j_2 \in \Omega_{CL},\ j_1 \ne j_2$) are both satisfied at any time $t \in [t_k, t_{k+1}]$ and*

$$\bigcap_{\substack{\beta \in [0,1] \\ l_1 \in \mathcal{V}_L^{j_1}, l_2 \in \mathcal{V}_L^{j_2}, j_1 \ne j_2}} \|\mathbf{r}_{l_1,HT}^{j_1} - \mathbf{r}_{l_2,HT}^{j_2}\| \ge \left(\delta^{j_1} + \delta^{j_2} + 2\epsilon\right). \tag{39}$$

Furthermore, assume privacy condition (29) is satisfied at all times t. Then, no two UAVs in clusters j_1 and j_2 collide.

Proof. If $\mathcal{C}_{col,k}^{j_1} \le 0$ and $\mathcal{C}_{col,k}^{j_2} \le 0$, then,

$$\forall l_1 \in \mathcal{V}^{j_1}, \qquad \|\mathbf{r}_{l_1}^{j_1} - \mathbf{r}_{l_1,HT}^{j_1}\| \le \delta^{j_1}, \tag{40a}$$

$$\forall l_2 \in \mathcal{V}^{j_2}, \qquad \|\mathbf{r}_{l_2}^{j_2} - \mathbf{r}_{l_2,HT}^{j_2}\| \le \delta^{j_2}, \tag{40b}$$

and the following statements are true:

1. Inter-agent collision avoidance is guaranteed in cluster j_u ($u = 1, 2$).
2. No follower UAV leaves leading triangle j_u ($u = 1, 2$).

Furthermore, cluster $j_1 \in \Omega_{CL}$ is not trespassed by a UAV from cluster j_2, if privacy condition (29) is satisfied. UAV $l_1 \in \mathcal{V}^{j_1}$ never collides with UAV $l_2 \in \mathcal{V}^{j_2}$ if leaders of clusters j_1 and j_2 do not collide. By considering Eq. (40),

$$\left\|\mathbf{r} - \mathbf{r}_{l_1,HT}^{j_1}\right\| \le \delta^{j_1} + \epsilon,$$

$$\left\|\mathbf{r} - \mathbf{r}_{l_2,HT}^{j_2}\right\| \le \delta^{j_2} + \epsilon$$

are the safe zones of leaders $l_1 \in \mathcal{V}_L^{j_1}$ and $l_2 \in \mathcal{V}_L^{j_2}$ and must not be trespassed by any UAV. Collision avoidance between leaders $l_1 \in \mathcal{V}_L^{j_1}$ and $l_2 \in \mathcal{V}_L^{j_2}$ is guaranteed if inequality (39) is satisfied. □

Definition 1 *(Valid deformation).* Define current configurations $\bar{\mathbf{T}}_c^{j_1} = (\mathbf{P}_{1,c}^{j_1}, \mathbf{P}_{2,c}^{j_2}, \mathbf{P}_{3,c}^{j_2})$ and $\bar{\mathbf{T}}_c^{j_2} = (\mathbf{P}_{1,c}^{j_2}, \mathbf{P}_{2,c}^{j_2}, \mathbf{P}_{3,c}^{j_2})$ and next configurations $\bar{\mathbf{T}}_n^{j_1} = (\mathbf{P}_{1,n}^{j_1}, \mathbf{P}_{2,n}^{j_2}, \mathbf{P}_{3,n}^{j_2})$ and $\bar{\mathbf{T}}_n^{j_2} = (\mathbf{P}_{1,n}^{j_2}, \mathbf{P}_{2,n}^{j_2}, \mathbf{P}_{3,n}^{j_2})$. Assume leader $l_u \in \mathcal{V}_{j_u}$ ($u = 1$) moves along a straight path connecting $\mathbf{P}_{l_u,c}^{j_u}$ and $\mathbf{P}_{l_u,n}^{j_u}$ as defined by Eq. (34):

$$u = 1, 2,\ l_u \in \mathcal{V}_L^{j_u}, \qquad \mathbf{r}_{l_u,HT}^{j_u} = (1 - \beta)\,\mathbf{P}_{l_u,c}^{j_u} + \beta \mathbf{P}_{l_u,n}^{j_u} + z_{HT}\hat{\mathbf{e}}_3.$$

Evolution of leading triangle j_u is called a ***valid deformation*** if

1. $\mathbf{P}_{l,n}^{j_u}$ is defined by Eq. (33) and
2. Containment and collision avoidance condition (38), privacy condition (29), obstacle avoidance condition (30) and inequality constraint (39) are satisfied at any $\beta \in [0, 1]$.

5.2. Cluster deformation optimization

We apply A* search to optimally plan the multi-cluster continuum deformation leader waypoints given clusters' initial and target configurations. To set up the path-planning problem, we define the following symbols:

$$s_0 = \left(\bar{\mathbf{T}}_0^1, \cdots, \bar{\mathbf{T}}_0^m\right) := \text{Initial node}$$

$$s_g = \left(\bar{\mathbf{T}}_g^1, \cdots, \bar{\mathbf{T}}_g^m\right) := \text{Goal node}$$

$$s_c = \left(\bar{\mathbf{T}}_c^1, \cdots, \bar{\mathbf{T}}_c^m\right) := \text{Current node}$$

$$s_n = \left(\bar{\mathbf{T}}_n^1, \cdots, \bar{\mathbf{T}}_n^m\right) := \text{Next node}$$

Note that s_n is a valid continuum deformation. Superscripts $1, \cdots, m$ denote cluster index numbers. Cluster leaders' optimal paths are assigned by minimizing deformation cost

$$f(s_n) = g(s_n) + h(s_n), \tag{41}$$

where $h(s_n)$ is the admissible heuristic cost assigned as follows:

$$h(s_n) = \sqrt{\sum_{\forall j} \sum_{l \in \mathcal{V}_L^j} \left\|\mathbf{P}_{l,n}^j - \mathbf{P}_{l,g}^j\right\|^2}, \tag{42}$$

Note that $h(s_n)$ is the sum of leaders' straight line distances from their target destinations. Furthermore, $g(s_n)$ is the minimum estimated cost from s_0 to s_n

$$g(s_n) = \min\left\{g(s_c) + C_{c,n}\right\}, \tag{43}$$

where

$$C_{c,n} = \sqrt{\sum_{\forall j} \sum_{l \in \mathcal{V}_L^j} \left\|\mathbf{P}_{l,n}^j - \mathbf{P}_{l,c}^j\right\|^2}. \tag{44}$$

5.3. Leader trajectory planning

Leaders' paths are all piecewise linear. To ensure that leaders' trajectories are $\mathcal{C}^2$ continuous, β in Eq. (34) is given by a fifth order polynomial:

$$t \in [t_{k-1}, t_k], \qquad \beta(t) = \sum_{i=0}^{5} = a_{i,k} t^{5-i}, \tag{45}$$

subject to

$$\begin{aligned} \beta\left(t_{k-1}\right) &= 0, \\ \beta\left(t_{k-1}\right) &= 1, \\ \dot{\beta}\left(t_{k-1}\right) &= \dot{\beta}\left(t_k\right) = 0, \\ \ddot{\beta}\left(t_{k-1}\right) &= \ddot{\beta}\left(t_k\right) = 0 \end{aligned} \tag{46}$$

Assuming $\Delta t = t_k - t_{k-1}$ ($\forall k$), $a_{0,k}$ through $a_{5,k}$ are determined by solving the following linear equality constraints:

$$\begin{bmatrix} 0 & 0 & 0 & 0 & 0 & 1 \\ \Delta t^5 & \Delta t^4 & \Delta t^3 & \Delta t^2 & \Delta t & 1 \\ 0 & 0 & 0 & 0 & 1 & 0 \\ 5\Delta t^4 & 4\Delta t^3 & 3\Delta t^2 & 2\Delta t & 1 & 0 \\ 0 & 0 & 0 & 2 & 0 & 0 \\ 20\Delta t^3 & 12\Delta t^2 & 6\Delta t & 2 & 0 & 0 \end{bmatrix} \begin{bmatrix} a_{0,k} \\ a_{1,k} \\ a_{2,k} \\ a_{3,k} \\ a_{4,k} \\ a_{5,k} \end{bmatrix} = \begin{bmatrix} 0 \\ 1 \\ 0 \\ 0 \\ 0 \\ 0 \end{bmatrix}. \tag{47}$$

5.4. Follower coordination planning

Leaders' global and local desired positions are the same and defined by Eq. (34) given current and new waypoints assigned by A*. Knowing leaders' desired trajectories, UAV desired trajectories are assigned using Eq. (4).

6. Quadcopter dynamics and control

Dynamics: Define UAV $i \in \mathcal{V}^j$ centroid position $\mathbf{r}_i^j = [x_i^j \ y_i^j \ z_i^j]^T$, Euler angles ϕ_i^j, θ_i^j, and ψ_i^j, mass m_i^j, and thrust force $F_{T,i}^j$. The dynamics of UAV $i \in \mathcal{V}_F^j$ is given by

$$\begin{aligned} \dot{\mathbf{r}}_i^j &= \mathbf{v}_i^j \\ \dot{\mathbf{v}}_i^j &= \begin{bmatrix} 0 & 0 & -g \end{bmatrix}^T + \bar{F}_{T,i}^j \hat{\mathbf{k}}_{b,i}^j \ . \\ \begin{bmatrix} \ddot{\bar{F}}_{T,i}^j & \ddot{\phi}_i^j & \ddot{\theta}_i^j & \ddot{\psi}_i^j \end{bmatrix}^T &= \begin{bmatrix} u_{T,i}^j & u_{\phi,i}^j & u_{\theta,i}^j & u_{\psi,i}^j \end{bmatrix}^T \end{aligned} \tag{48}$$

Note that gravity $g = 9.81 \frac{m}{s^2}$ and $\bar{F}_{T,i}^j = \frac{F_{T,i}^j}{m_i^j}$ is thrust force per mass m_i^j, and $\hat{\mathbf{k}}_{b,i}^j$ is the thrust direction unit vector $\bar{F}_{T,i}^j$. Dynamics (48) can be rewritten in the following form:

$$\begin{cases} \dot{\mathcal{X}}_i^j = \mathbf{F}_i^j\left(\mathcal{X}_i^j\right) + \mathbf{G}\mathcal{V}_i^j \\ \mathbf{r}_i^j = h_i^j\left(\mathcal{X}_i^j\right) = [x_i^j \ y_i^j \ z_i^j]^T \end{cases}, \tag{49}$$

where

$$\mathcal{X}_i^j = [x_i^j \ y_i^j \ z_i^j \ v_{x,i}^j \ v_{y,i}^j \ v_{z,i}^j \ \bar{F}_{T,i}^j \ \phi_i^j \ \theta_i^j \ \psi_i^j \ \dot{\bar{F}}_{T,i}^j \ \dot{\phi}_i^j \ \dot{\theta}_i^j \ \dot{\psi}_i^j]^T$$

is the control state, $\mathbf{r}_i^j$ is the control output, $\mathbf{V}_i^j = [u_{T,i}^j \ u_{\phi,i}^j \ u_{\theta,i}^j]$ is the control input vector.

$$\begin{aligned} \mathbf{F}_i^j &= [v_{x,i}^j \ v_{y,i}^j \ v_{z,i}^j \ f_{4,i}^j \ f_{5,i}^j \ f_{6,i}^j \ \dot{\bar{F}}_{T,i}^j \ \dot{\phi}_i^j \ \dot{\theta}_i^j \ \dot{\psi}_i^j \ 0 \ 0 \ 0 \ f_{14,i}^j]^T \\ \begin{bmatrix} f_{4,i}^j \\ f_{5,i}^j \\ f_{6,i}^j \end{bmatrix} &= \begin{bmatrix} 0 \\ 0 \\ -g \end{bmatrix} + \bar{F}_{T,i}^j \begin{bmatrix} C_{\phi_i^j} S_{\theta_i^j} C_{\psi_i^j} + S_{\phi_i^j} S_{\psi_i^j} \\ C_{\phi_i^j} S_{\theta_i^j} S_{\psi_i^j} - S_{\phi_i^j} C_{\psi_i^j} \\ C_{\phi_i^j} C_{\theta_i^j} \end{bmatrix}, \end{aligned} \tag{50a}$$

$$\mathbf{G} = \begin{bmatrix} \mathbf{0}_{9\times 3} \\ \mathbf{I}_3 \\ \mathbf{0}_{2\times 3} \end{bmatrix}. \tag{50b}$$

Internal Dynamics (Yaw Control): This paper chooses $\ddot{\psi}_i^j = u_{\psi,i}^j = f_{14,i}^j$ as follows:

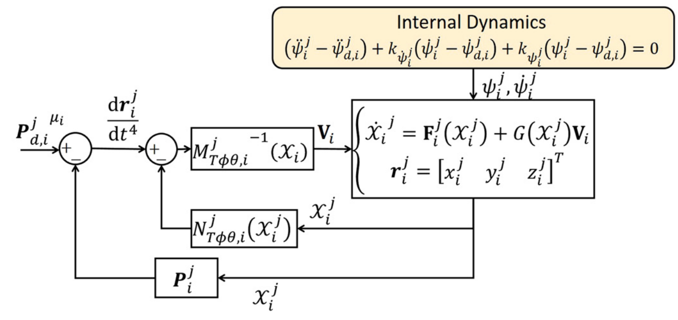

Fig. 5. UAV controller block diagram.

$$u_{\psi,i}^j = f_{14,i}^j = \ddot{\psi}_{d,i}^j + k_{\dot{\psi}_i^j}\left(\dot{\psi}_{d,i}^j - \ddot{\psi}_i^j\right) + k_{\psi_i^j}\left(\dot{\psi}_{d,i}^j - \ddot{\psi}_i^j\right),$$

where $k_{\psi_i^j}$ and $k_{\dot{\psi}_i^j}$ are positive constants and $\psi_{d,i}^j$, $\dot{\psi}_{d,i}^j$, and $\ddot{\psi}_{d,i}^j$ are known. Therefore, ψ_i^j is updated by the following stable second order dynamics (Fig. 5):

$$\left(\ddot{\psi}_i^j - \ddot{\psi}_{d,i}^j\right) + k_{\dot{\psi}_i^j}\left(\dot{\psi}_i^j - \dot{\psi}_{d,i}^j\right) + k_{\psi_i^j}\left(\psi_i^j - \psi_{d,i}^j\right) = 0. \tag{51}$$

Control: Defining the state transition $\mathcal{X}_i^j \to \left(\mathbf{r}_i^j, \dot{\mathbf{r}}_i^j, \ddot{\mathbf{r}}_i^j, \dddot{\mathbf{r}}_i^j, \psi_i^j, \dot{\psi}_i^j\right)$, UAV dynamics (49) is feedback linearizable and can be expressed as follows:

$$\begin{cases} \dfrac{d^4\mathbf{r}_i^j}{dt^4} = \mathbf{U}_i^j \\ \dfrac{d^2\psi_i^j}{dt^2} = \ddot{\psi}_{d,i}^j + k_{\dot{\psi}_i^j}\left(\dot{\psi}_{d,i}^j - \ddot{\psi}_i^j\right) + k_{\psi_i^j}\left(\dot{\psi}_{d,i}^j - \ddot{\psi}_i^j\right). \end{cases} \tag{52}$$

With feedback linearization, the UAV internal dynamics, assigned by the second row of Eq. (52), is asymptotically stable. Therefore, UAV dynamics (52) is stable, if $\mathbf{r}_i^j$ asymptotically tracks $\mathbf{r}_{d,i}^j = [x_{d,i}^j \ y_{d,i}^j \ z_{d,i}^j]$. Note that $x_{d,i}^j$, $y_{d,i}^j$, and $z_{d,i}^j$ are the components of the local desired position of UAV $i \in \mathcal{V}^j$ defined by Eq. (4). The first equation of (52) can be expressed as follows:

$$\frac{d^4\mathbf{r}_i^j}{dt^4} = M_{T\phi\theta,i}^j \mathbf{V}_i^j + \mathbf{N}_{T\phi\theta,i}^j, \tag{53}$$

where

$$\mathbf{M}_{T\phi\theta,i}^j = \begin{bmatrix} \Lambda_{1,i}^j & \Lambda_{2,i}^j & \Lambda_{3,i}^j \end{bmatrix}, \tag{54a}$$

$$\mathbf{N}_{T\phi\theta,i}^j = \dot{\Lambda}_{0,i}^j + \dot{\Lambda}_{1,i}^j \dot{\bar{F}}_{T,i}^j + \dot{\Lambda}_{2,i}^j \dot{\phi}_i^j + \dot{\Lambda}_{3,i}^j \dot{\theta}_{T,i}^j, \tag{54b}$$

$$\Lambda_{0,i}^j = \dot{\psi}_i^j \begin{bmatrix} -C_{\phi_i}^j S_{\theta_i}^j S_{\psi_i}^j + S_{\phi_i}^j C_{\psi_i}^j \\ C_{\phi_i}^j S_{\theta_i}^j C_{\psi_i}^j + S_{\phi_i}^j S_{\psi_i}^j \\ 0 \end{bmatrix}, \tag{54c}$$

$$\Lambda_{1,i}^j = \begin{bmatrix} C_{\phi_i}^j S_{\theta_i}^j C_{\psi_i}^j + S_{\phi_i}^j S_{\psi_i}^j \\ C_{\phi_i}^j S_{\theta_i}^j S_{\psi_i}^j - S_{\phi_i}^j C_{\psi_i}^j \\ C_{\phi_i}^j C_{\theta_i}^j \end{bmatrix}, \tag{54d}$$

$$\Lambda_{2,i}^j = \begin{bmatrix} -S_{\phi_i}^j S_{\theta_i}^j C_{\psi_i}^j + C_{\phi_i}^j S_{\psi_i}^j \\ -S_{\phi_i}^j S_{\theta_i}^j S_{\psi_i}^j - C_{\phi_i}^j C_{\psi_i}^j \\ -S_{\phi_i}^j C_{\theta_i}^j \end{bmatrix}, \tag{54e}$$

$$\Lambda_{3,i}^j = \begin{bmatrix} C_{\phi_i}^j C_{\theta_i}^j C_{\psi_i}^j \\ C_{\phi_i}^j C_{\theta_i}^j S_{\psi_i}^j \\ -S_{\theta_i}^j C_{\phi_i}^j \end{bmatrix}. \tag{54f}$$

Equating right-hand sides of Eq. (53) and the first row of Eq. (52), $\mathbf{U}_i^j$ and $\mathbf{V}_i^j$ are related by

$$\mathbf{V}_i^j = {\mathbf{M}_{T\phi\theta,i}^j}^{-1}\left(\mathbf{U}_i^j - \mathbf{N}_{T\phi\theta,i}^j\right). \tag{55}$$

Let $\mathbf{U}_i^j$ be chosen as follows:

$$\mathbf{U}_i^j = {\mathbf{P}_{d,i}^j}^{\mu_i} - \mathbf{P}_i^j, \tag{56}$$

where

$$\mathbf{P}_i^j = \sum_{l=1}^{4}\gamma_l^j \frac{\mathrm{d}^{4-j}\mathbf{r}_i^j}{\mathrm{d}t}, \tag{57a}$$

$${\mathbf{P}_{d,i}^j}^{\mu_i} = \sum_{l=0}^{\mu_i}\gamma_{4-l}^j \frac{\mathrm{d}^l\mathbf{r}_{d,i}^j}{\mathrm{d}t}, \tag{57b}$$

$$\forall j \in \Omega_{CL}, \qquad \mu_i = \begin{cases} 4 & i \in \mathcal{V}_L^j \\ 3 & i \in \mathcal{V}_F^j \end{cases}, \tag{57c}$$

where $\gamma_1^j, \gamma_2^j, \gamma_3^j, \gamma_4^j > 0$ are appropriately chosen such that the MUS collective dynamics is stable. Stability of MUS collective dynamics is discussed in Theorem 3.

Define

$$\begin{aligned}
q &= x, y, z, & \mathcal{Z}_q^j &= [q_1^j \ \cdots \ q_{N_j}^j]^T, \\
q &= x, y, z, & \mathcal{Z}_{q,L} &= [q_1^j \ q_2^j \ q_3^j]^T, \\
q &= x, y, z, & \mathcal{Z}_{q,F} &= [q_4^j \ \cdots \ q_{N_j}^j]^T, \\
q &= x, y, z, & \mathcal{Z}_{\mathrm{MUS},q}^j &= \begin{bmatrix} \mathcal{Z}_q^{j^T} & \dot{\mathcal{Z}}_q^{j^T} & \ddot{\mathcal{Z}}_q^{j^T} & \dddot{\mathcal{Z}}_q^{j^T} \end{bmatrix}^T, \\
q &= x, y, z, & \mathbf{U}_{\mathrm{MUS},q}^j &= \frac{\mathrm{d}^4\mathcal{Z}_{q,L,HT}^j}{\mathrm{d}t^4}.
\end{aligned} \tag{58}$$

If position of follower $i \in \mathcal{V}^j$ is updated according to Eq. (56), then, collective dynamics of cluster j is expressed by

$$\frac{\mathrm{d}^4\mathcal{Z}_{q,L}^j}{\mathrm{d}t^4} = \frac{\mathrm{d}^4\mathcal{Z}_{q,L,HT}^j}{\mathrm{d}t^4} + \sum_{l=1}^{4}\gamma_l^j \frac{\mathrm{d}^{4-l}\left(\mathcal{Z}_{q,L,HT}^j - \mathcal{Z}_{q,L}^j\right)}{\mathrm{d}t^{4-l}}, \tag{59a}$$

$$\frac{\mathrm{d}^4\mathcal{Z}_{q,F}^j}{\mathrm{d}t^4} = \sum_{l=1}^{4}\gamma_l^j\mathbf{A}^j \frac{\mathrm{d}^{4-l}\mathcal{Z}_{q,F}^j}{\mathrm{d}t^{4-l}} + \sum_{l=1}^{4}\gamma_l^j\mathbf{B}^j \frac{\mathrm{d}^{4-l}\mathcal{Z}_{L,q}^j}{\mathrm{d}t^{4-j}}. \tag{60}$$

Collective dynamics (59) can be rewritten in the following state-space form:

$$q = x, y, z, \qquad \dot{\mathcal{Z}}_{\mathrm{MUS},q}^j = \mathbf{A}_{\mathrm{SYS}}^j \mathcal{Z}_{\mathrm{MUS},q}^j + \mathbf{B}_{\mathrm{SYS}}^j \mathbf{U}_{\mathrm{MUS},q}^j, \tag{61}$$

where

$$\mathbf{A}_{\mathrm{SYS}}^j = \begin{bmatrix} \mathbf{0}_{N_j} & \mathbf{I}_{N_j} & \mathbf{0}_{N_j} & \mathbf{0}_{N_j} \\ \mathbf{0}_{N_j} & \mathbf{0}_{N_j} & \mathbf{I}_{N_j} & \mathbf{0}_{N_j} \\ \mathbf{0}_{N_j} & \mathbf{0}_{N_j} & \mathbf{0}_{N_j} & \mathbf{I}_{N_j} \\ \gamma_4^j\mathbf{A}_{\mathrm{MUS}}^j & \gamma_3^j\mathbf{A}_{\mathrm{MUS}}^j & \gamma_2^j\mathbf{A}_{\mathrm{MUS}}^j & \gamma_1^j\mathbf{A}_{\mathrm{MUS}}^j \end{bmatrix} \tag{62a}$$

$$\mathbf{A}_{\mathrm{MUS}}^j = \begin{bmatrix} -\mathbf{I}_3 & \mathbf{0}_{3\times(N_j-3)} \\ \mathbf{B}^j & \mathbf{A}^j \end{bmatrix}, \tag{62b}$$

$$\mathbf{A}_{\mathrm{SYS}}^j = \begin{bmatrix} \mathbf{0}_{3\times 3N_j} & \mathbf{I}_3 & \mathbf{0}_{3\times(N_j-3)} \end{bmatrix}^T. \tag{62c}$$

Note that $\mathbf{0}_{N_j} \in \mathbb{R}^{N_j\times N_j}$ and $\mathbf{0}_{3\times(N_j-3)} \in \mathbb{R}^{3\times(N_j-3)}$ are zero-entry matrices and I_3 and I_{N_j} are identity matrices.

Theorem 3. *Define $\mathbf{E}_{q,L}^j = \mathcal{Z}_{q,L}^j - \mathcal{Z}_{q,L,HT}^j$ and $\mathbf{E}_{q,F}^j = \mathcal{Z}_{q,F}^j - \mathcal{Z}_{q,F,HT}^j$ as the error signals specifying deviation of cluster j leader and follower UAVs from global desired positions given by (10). If the position of UAV $i \in \mathcal{V}^j$ is updated according to dynamics in (52) and (56), then the following statements hold:*

- *The error signals $\mathbf{E}_{q,L}^j$ and $\mathbf{E}_{q,F}^j$ ($j \in \Omega_{CL}$, $q = x, y, z$) are updated by the following fourth order dynamics:*

$$\frac{\mathrm{d}^4\mathbf{E}_{q,L}^j}{\mathrm{d}t^4} = \sum_{l=1}^{4}\gamma_l^j \frac{\mathrm{d}^{4-l}\left(\mathbf{E}_{q,L}^j\right)}{\mathrm{d}t^{4-l}}, \tag{63a}$$

$$\frac{\mathrm{d}^4\mathbf{E}_{q,F}^j}{\mathrm{d}t^4} = \sum_{l=1}^{4}\gamma_l^j\left(\boldsymbol{A}^j\frac{\mathrm{d}^{4-j}\mathbf{E}_{q,F}^j}{\mathrm{d}t^{4-j}} + \boldsymbol{B}^j\frac{\mathrm{d}^{4-l}\mathbf{E}_{q,L}^j}{\mathrm{d}t^{4-l}}\right) - \boldsymbol{W}_L^j\frac{\mathrm{d}^4\mathcal{Z}_{q,L,HT}^j}{\mathrm{d}t^4}. \tag{63b}$$

- *Error dynamics (63a) and (63b) are asymptotically stable, if $\left|s^4\mathbf{I}_{N_j-3} - \sum_{l=0}^{3}s^l\gamma_{4-l}^j\boldsymbol{A}^j\right| = 0$, roots are all located in the left-hand side of the s-plane.*

Proof. By subtracting $\frac{\mathrm{d}^4\mathcal{Z}_{L,q,HT}^j}{\mathrm{d}t^4}$ from both sides of Eq. (59a), Eq. (59a) can be rewritten as Eq. (63a) and (60) becomes

$$\frac{\mathrm{d}^4\mathcal{Z}_{q,F}}{\mathrm{d}t^4} = \sum_{l=1}^{4}\gamma_l^j\left(\mathbf{A}^j\frac{\mathrm{d}^{4-l}\mathcal{Z}_{q,F}^j}{\mathrm{d}t^{4-l}} + \mathbf{B}^j\frac{\mathrm{d}^{4-l}\mathcal{Z}_{q,L,HT}^j}{\mathrm{d}t^{4-l}} + \mathbf{B}^j\frac{\mathrm{d}^{4-l}\mathbf{E}_{q,L}^j}{\mathrm{d}t^{4-l}}\right). \tag{64}$$

Substituting $\mathbf{B} = -\mathbf{A}\mathbf{W}_L$, Eq. (64) can be rewritten as follows:

$$\frac{\mathrm{d}^4\mathcal{Z}_{q,F}^j}{\mathrm{d}t^4} = \sum_{l=1}^{4}\gamma_l^j\mathbf{A}^j\frac{\mathrm{d}^{4-l}\mathbf{E}_{q,F}}{\mathrm{d}t^{4-l}} + \sum_{l=1}^{4}\gamma_l^j\mathbf{B}^j\frac{\mathrm{d}^{4-j}\mathbf{E}_{L,q}}{\mathrm{d}t^{4-j}}. \tag{65}$$

By subtracting $\frac{\mathrm{d}^4\mathbf{Z}_{q,F,HT}}{\mathrm{d}t^4} = \mathbf{W}_L\frac{\mathrm{d}^4\mathcal{Z}_{q,L,HT}}{\mathrm{d}t^4}$ from both sides of Eq. (65), $\mathbf{E}_{F,q}$ is updated by Eq. (63b). Note that the error dynamics (63b) is asymptotically stable if the roots of the error characteristic equation,

$$j \in \Omega_{CL}, \qquad \left|s^4 I_{N_j-3} - \sum_{l=0}^{3}s^l\gamma_{4-l}^j\mathbf{A}^j\right| = 0,$$

are all located in the left-half s-plane. □

7. Simulation results

Consider an MUS consisting of two clusters ($\Omega_{CL} = \{1, 2\}$, $m = 2$ with initial configurations shown in Fig. 6. Each cluster consists of 18 UAVs ($N_1 = N_2 = 18$). Leader UAVs are identified by local index numbers 1, 2, and 3, and follower UAVs are locally indexed by 4, $\cdots$, 18. As shown in Fig. 7, leaders of clusters 1 and 2 are initially placed at $\mathbf{r}_{1,0}^1 = 10\hat{\mathbf{e}}_1 + 10\hat{\mathbf{e}}_2 + 10\hat{\mathbf{e}}_3$, $\mathbf{r}_{2,0}^1 = 40\hat{\mathbf{e}}_1 + 30\hat{\mathbf{e}}_2 + 10\hat{\mathbf{e}}_3$, $\mathbf{r}_{3,0}^1 = 10\hat{\mathbf{e}}_1 + 50\hat{\mathbf{e}}_2 + 10\hat{\mathbf{e}}_3$, $\mathbf{r}_{1,0}^2 = 100\hat{\mathbf{e}}_1 + 10\hat{\mathbf{e}}_2 + 10\hat{\mathbf{e}}_3$, $\mathbf{r}_{2,0}^2 = 100\hat{\mathbf{e}}_1 + 40\hat{\mathbf{e}}_2 + 10\hat{\mathbf{e}}_3$, and $\mathbf{r}_{3,0}^2 = 70\hat{\mathbf{e}}_1 + 30\hat{\mathbf{e}}_2 + 10\hat{\mathbf{e}}_3$.

Followers' Evolution: Communication graphs shown in Fig. 6 define inter-agent communication among UAVs in clusters 1 and 2. Given initial positions (shown in Fig. 6), communication weights are computed using Eq. (21). For instance, UAV 17 communicates with in-neighbor UAVs 11, 13, and 16 in cluster 1, where $\mathbf{r}_{17,0}^1 =$

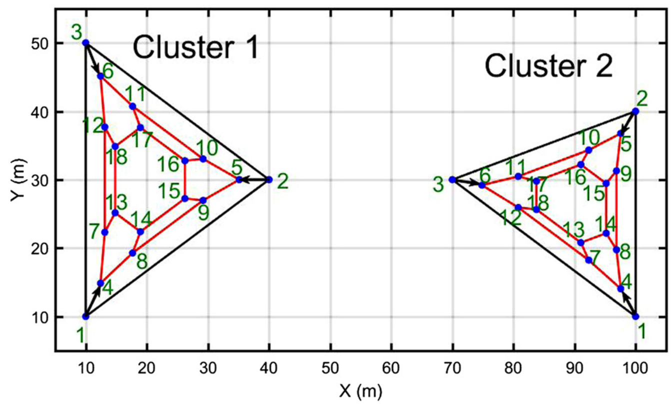

Fig. 6. Initial configurations of clusters 1 and 2. This figure also shows graphs defining inter-agent communication for clusters 1 and 2.

$18.9548\hat{\mathbf{e}}_1 + 37.6103\hat{\mathbf{e}}_2$, $\mathbf{r}^1_{17,0} = 17.6720\hat{\mathbf{e}}_1 + 40.7236\hat{\mathbf{e}}_2$, $\mathbf{r}^1_{17,0} = 14.8149\hat{\mathbf{e}}_1 + 25.1496\hat{\mathbf{e}}_2$, and $\mathbf{r}^1_{17,0} = 26.2303\hat{\mathbf{e}}_1 + 32.7599\hat{\mathbf{e}}_2$. Therefore, communication weights $w^1_{17,11}$, $w^1_{17,13}$, and $w^1_{17,16}$ are obtained as follows:

$$\begin{bmatrix} 17.6720 & 14.8149 & 26.2303 \\ 40.7236 & 25.1496 & 32.7599 \\ 1 & 1 & 1 \end{bmatrix}^{-1} \begin{bmatrix} 18.9548 \\ 14.8149 \\ 1 \end{bmatrix} = \begin{bmatrix} 0.55 \\ 0.225 \\ 0.225 \end{bmatrix}$$

Follower communication weights calculated by Eq. (21) are as follows:

$$j \in \Omega_{CL}, \qquad \begin{aligned} w^j_{4,1} =& w^j_{5,2} = w^j_{6,3} = w^j_{7,4} = w^j_{8,4} = w^j_{9,5} = w^j_{10,5} \\ =& w^j_{11,6} = w^j_{13,7} = w^j_{14,8} = w^j_{15,9} = w_{16,10} \\ =& w^j_{17,11} = w^j_{18,12} = 0.55. \end{aligned}$$

The remaining communication weights are all 0.225. UAVs all choose $\gamma^j_1 = 30.9375$, $\gamma^j_2 = 52.8438$, $\gamma^j_3 = 33.6875$, and $\gamma^j_4 = 9.5000$ ($j \in \Omega_{CL} = \{1, 2\}$).

Inter-agent Collision Avoidance Verification: We choose $\lambda^j_{\mathrm{CD,min}} = 0.5$ ($j \in \Omega_{CL} = \{1, 2\}$). In cluster $1 \in \Omega_{CL}$, UAVs $9 \in \mathcal{V}^1_F$ and $15 \in \mathcal{V}^1_F$ have the minimum separation distance $d^1_s = 2.989m$ at the initial time. Furthermore, UAV $6 \in \mathcal{V}^1_F$ is at the closest distance from the boundary of the leading triangle $1 \in \Omega_{CL}$. In cluster $2 \in \Omega_{CL}$, UAVs $10 \in \mathcal{V}^2_F$ and $16 \in \mathcal{V}^2_F$ have minimum separation distance $d^2_s = 2.4789m$ at the initial time. Moreover, UAV $6 \in \mathcal{V}^2_F$ is at the closest distance $d^2_b = 2.0206m$ from sides $1-3$ of leading triangle $2 \in \Omega_{CL}$. We assume each UAV can be enclosed by a ball with radius $\epsilon = 0.5m$. Using Eq. (35),

$$\begin{aligned} \delta^1_{max} =& \min\left\{\frac{1}{2}\left(d^1_s - 2\epsilon\right), \left(d^1_b - \epsilon\right)\right\} = 0.9944m \\ \delta^2_{max} =& \min\left\{\frac{1}{2}\left(d^2_s - 2\epsilon\right), \left(d^2_b - \epsilon\right)\right\} = 0.7395m \end{aligned}.$$

Therefore, $\delta^1 = 0.2472m$ and $\delta^2 = 0.1198m$ assign upper limits for UAV deviations in clusters 1 and 2, respectively, such that $\|\mathbf{r}_i(t) - \mathbf{r}_{i,HT}(t)\| \leq \delta^j_i$, $j \in \Omega_{CL} = \{1, 2\}$, $i \in \mathbf{V}^j = \{1, \cdots, 18\}$.

7.1. Case-study 1: limited airspace without no-flying zone

It is aimed that cluster leaders ultimately reach $\mathbf{r}^1_{1,F} = 100\hat{\mathbf{e}}_1 + 40\hat{\mathbf{e}}_2 + 10\hat{\mathbf{e}}_3$, $\mathbf{r}^1_{2,F} = 100\hat{\mathbf{e}}_1 + 70\hat{\mathbf{e}}_2 + 10\hat{\mathbf{e}}_3$, $\mathbf{r}^1_{3,F} = 70\hat{\mathbf{e}}_1 + 60\hat{\mathbf{e}}_2 + 10\hat{\mathbf{e}}_3$, $\mathbf{r}^2_{1,F} = 40\hat{\mathbf{e}}_1 + 10\hat{\mathbf{e}}_2 + 10\hat{\mathbf{e}}_3$, $\mathbf{r}^2_{2,F} = 40\hat{\mathbf{e}}_1 + 40\hat{\mathbf{e}}_2 + 10\hat{\mathbf{e}}_3$, and $\mathbf{r}^2_{3,F} = 10\hat{\mathbf{e}}_1 + 30\hat{\mathbf{e}}_2 + 10\hat{\mathbf{e}}_3$. The path of leader $i \in \mathcal{V}^j_L$ ($j \in \Omega_{CL} = \{1, 2\}$) must satisfy motion constraints, defined in Eq. (32), to ensure collective motion safety. Optimal leaders' waypoints are obtained using A* and listed in Table 1. Leaders' straight paths

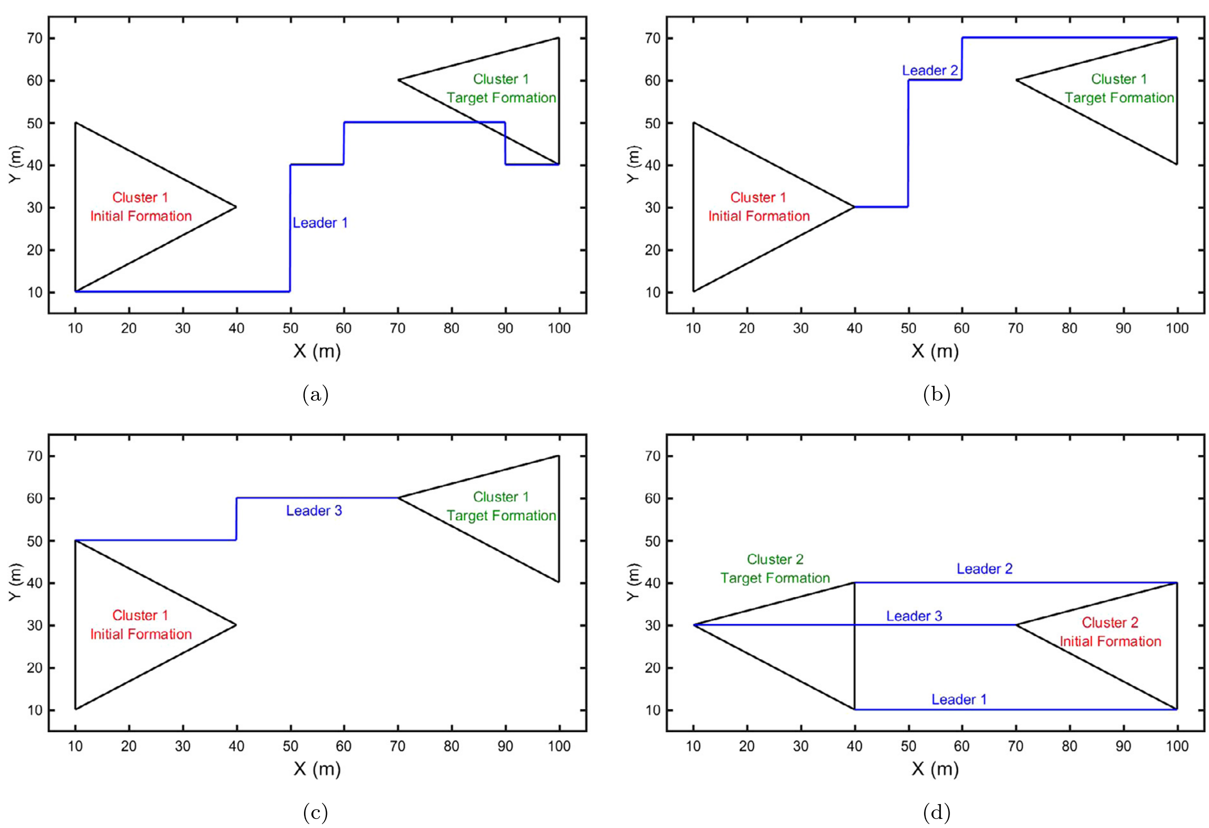

Fig. 7. Initial and target configurations of UAV clusters 1 and 2 in Case Study 1. (a-c) Optimal path for leaders guiding cluster 1. (d) Optimal path for leaders guiding cluster 2.

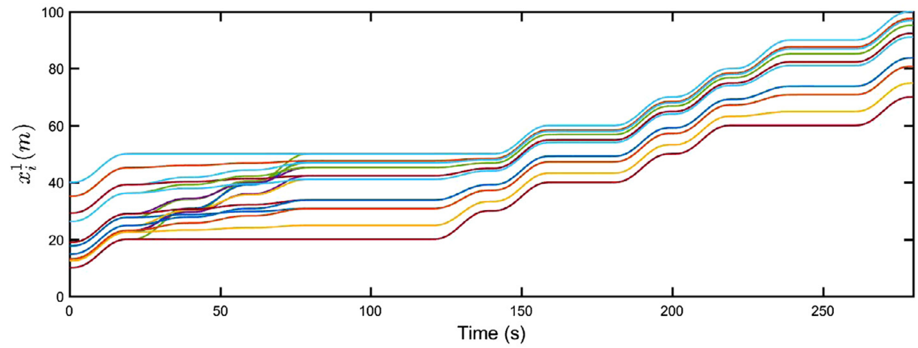

(a) x components of cluster 1

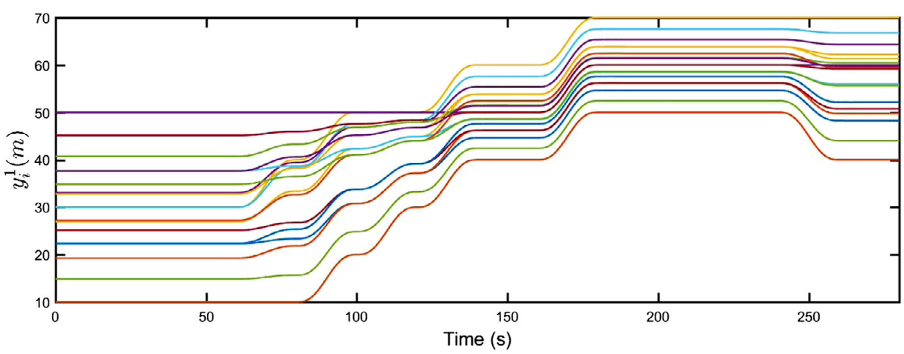

(b) y components of cluster 1

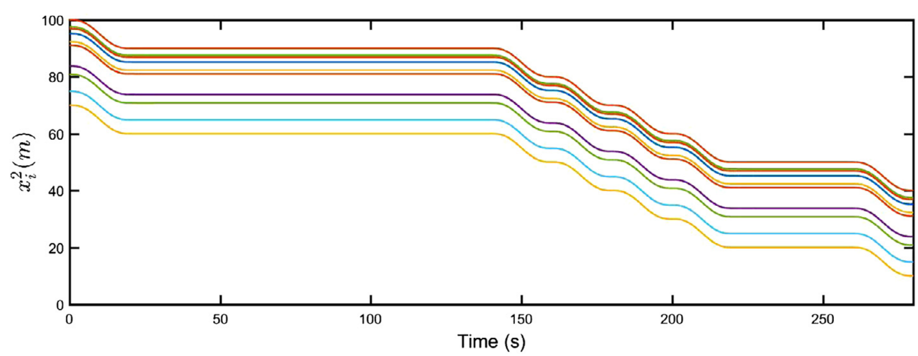

(c) x components of cluster 2

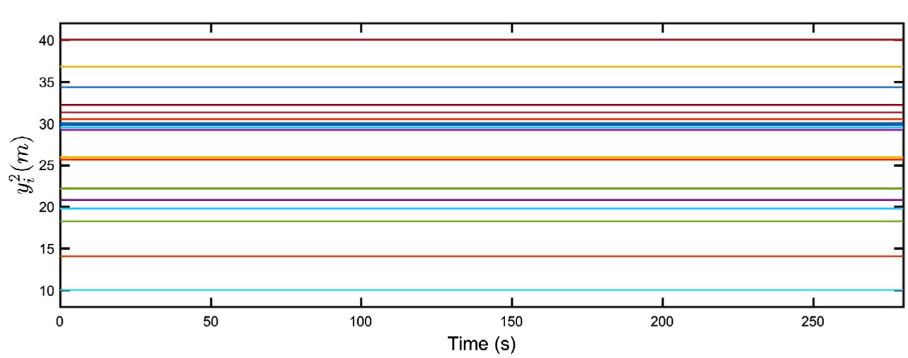

(d) y components of cluster 2

Fig. 8. Case-study 1: (a) x components of UAVs in cluster 1 versus time. (b) y components of UAVs in cluster 1 versus time. (c) x components of UAVs in cluster 2 versus time. (d) y components of UAVs in cluster 2 versus time.

Table 1
Optimal waypoints assigned by A* in case study 1.

Time	$\mathbf{P}^1_{1,c}(m)$	$\mathbf{P}^1_{2,c}(m)$	$\mathbf{P}^1_{3,c}(m)$	$\mathbf{P}^2_{1,c}(m)$	$\mathbf{P}^2_{2,c}(m)$	$\mathbf{P}^2_{3,c}(m)$
$t_0 = 0s$	(10, 10)	(40, 30)	(10, 50)	(100, 10)	(100, 40)	(70, 30)
$t_1 = 20s$	(20, 10)	(50, 30)	(20, 50)	(90, 10)	(90, 40)	(60, 30)
$t_2 = 40s$	(30, 10)	(50, 30)	(2050)	(90, 10)	(90, 40)	(60, 30)
$t_3 = 60s$	(40, 10)	(50, 30)	(20, 50)	(90, 10)	(90, 40)	(60, 30)
$t_4 = 80s$	(50, 10)	(50, 40)	(20, 50)	(9010)	(90, 40)	(60, 30)
$t_5 = 100s$	(50, 20)	(50, 50)	(20, 50)	(90, 10)	(90, 40)	(60, 30)
$t_6 = 120s$	(50, 30)	(50, 50)	(20, 50)	(90, 10)	(90, 40)	(60, 30)
$t_7 = 140s$	(50, 40)	(50, 60)	(30, 50)	(90, 10)	(90, 40)	(60, 30)
$t_8 = 160s$	(60, 40)	(60, 60)	(40, 50)	(80, 10)	(80, 40)	(50, 30)
$t_9 = 180s$	(60, 50)	(60, 70)	(40, 60)	(70, 10)	(70, 40)	(40, 30)
$t_{10} = 200s$	(70, 50)	(70, 70)	(50, 60)	(60, 10)	(60, 40)	(30, 30)
$t_{11} = 220s$	(80, 50)	(80, 70)	(60, 60)	(50, 10)	(50, 40)	(20, 30)
$t_{12} = 240s$	(90, 50)	(90, 70)	(60, 60)	(50, 10)	(50, 40)	(20, 30)
$t_{13} = 260s$	(90, 40)	(90, 70)	(60, 60)	(50, 10)	(50, 40)	(20, 30)
$t_{14} = 280s$	(100, 40)	(100, 70)	(70, 60)	(40, 10)	(40, 40)	(10, 30)

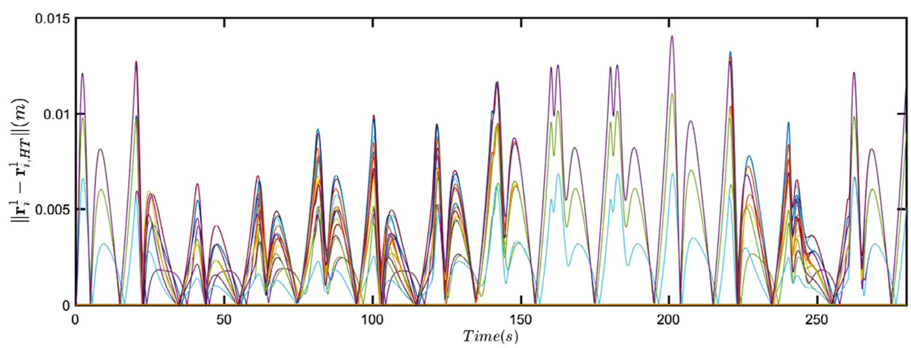

(a) Deviations of quadcopters in cluster 1

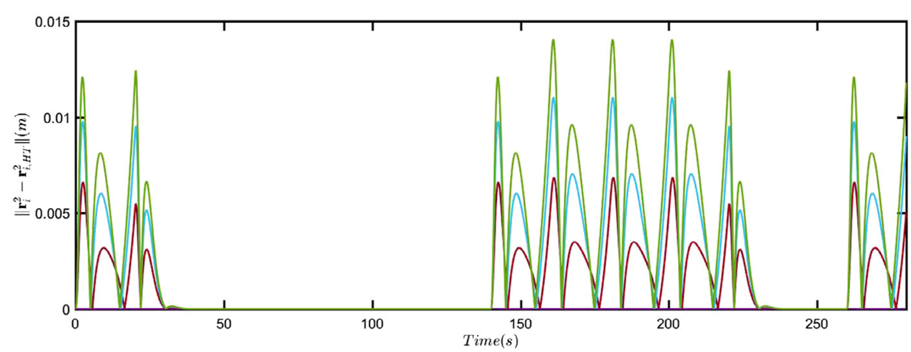

(b) Deviations of quadcopters in cluster 2

Fig. 9. Case-study 1: (a) Deviation of cluster 1 UAVs from global desired coordination. (b) Deviation of cluster 2 UAVs from global desired coordination.

Table 2
Optimal waypoints assigned by A* in case study 2.

Time	$\mathbf{P}^1_{1,c}(m)$	$\mathbf{P}^1_{2,c}(m)$	$\mathbf{P}^1_{3,c}(m)$	$\mathbf{P}^2_{1,c}(m)$	$\mathbf{P}^2_{2,c}(m)$	$\mathbf{P}^2_{3,c}(m)$
$t_0 = 0s$	(10, 10)	(40, 30)	(10, 50)	(100, 10)	(100, 40)	(70, 30)
$t_1 = 20s$	(20, 10)	(40, 30)	(10, 50)	(100, 10)	(100, 40)	(70, 30)
$t_2 = 40s$	(30, 10)	(40, 40)	(10, 50)	(100, 10)	(100, 40)	(70, 30)
$t_3 = 60s$	(40, 10)	(40, 50)	(10, 50)	(100, 10)	(100, 40)	(70, 30)
$t_4 = 80s$	(40, 20)	(50, 50)	(20, 50)	(100, 10)	(100, 40)	(70, 30)
$t_5 = 100s$	(50, 20)	(50, 60)	(30, 50)	(100, 10)	(100, 40)	(70, 30)
$t_6 = 120s$	(50, 30)	(60, 60)	(30, 60)	(90, 10)	(90, 40)	(60, 30)
$t_7 = 140s$	(50, 40)	(70, 60)	(40, 60)	(90, 10)	(90, 40)	(60, 30)
$t_8 = 160s$	(60, 40)	(70, 70)	(40, 70)	(80, 10)	(80, 40)	(50, 30)
$t_9 = 180s$	(70, 40)	(80, 70)	(50, 70)	(80, 10)	(80, 40)	(50, 30)
$t_{10} = 200s$	(70, 50)	(90, 70)	(60, 70)	(70, 10)	(70, 40)	(40, 30)
$t_{11} = 220s$	(70, 60)	(90, 80)	(60, 80)	(60, 10)	(60, 40)	(30, 30)
$t_{12} = 240s$	(70, 70)	(90, 90)	(60, 90)	(50, 10)	(50, 40)	(20, 30)
$t_{13} = 260s$	(80, 70)	(90, 90)	(60, 90)	(50, 10)	(50, 40)	(20, 30)
$t_{14} = 280s$	(90, 70)	(90, 100)	(60, 90)	(50, 10)	(50, 40)	(20, 30)
$t_{15} = 300s$	(100, 70)	(100, 100)	(70, 90)	(40, 10)	(40, 40)	(10, 30)

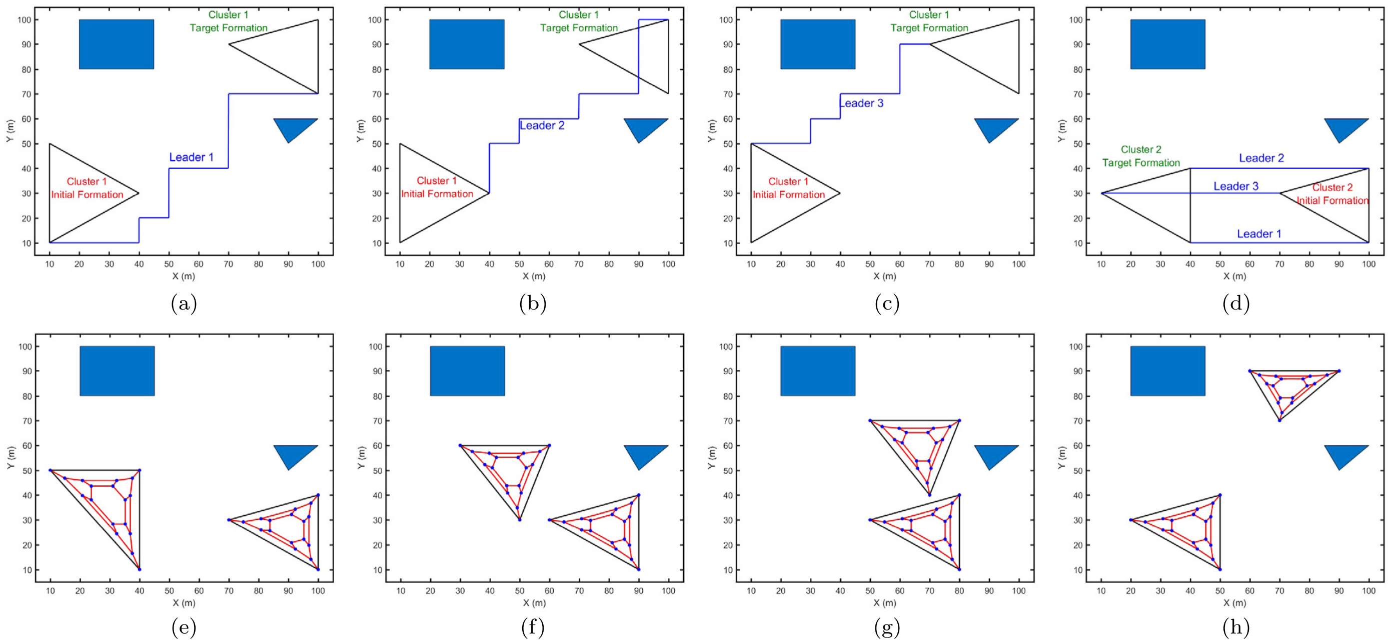

Fig. 10. (a-c) Optimal path for leaders guiding cluster 1 in Case Study 2. (d) Optimal path for leaders guiding cluster 2 in Case Study 2. (e-h) Cluster formations at $t = 60s$, $t = 120s$, $t = 180s$, and $t = 240s$.

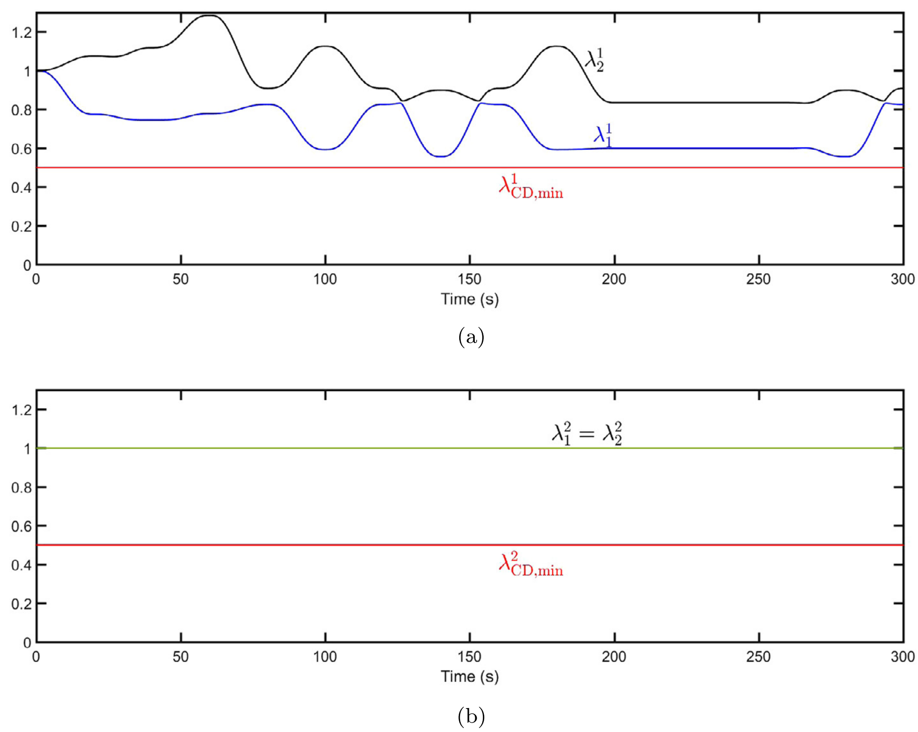

Fig. 11. Case-study 2: (a) Cluster 1 continuum deformation: Eigenvalues of matrix $\mathbf{U}_{CD}^1$, denoted by λ_1^1 and λ_2^1, versus time. (b) Cluster 2 continuum deformation: Eigenvalues of matrix $\mathbf{U}_{CD}^2$, denoted by λ_1^2 and λ_2^2, versus time.

connecting two consecutive waypoints are shown in Fig. 7. We choose $\Delta t = t_{k+1} - t_k = 20s$ $(k = 0, 1, \cdots, 13)$ such that $\mathbf{P}_{l,n}^j(t_k) = \mathbf{P}_{l,c}^j(t_{k+1})$, $i \in \mathcal{V}_L^j$, $j \in \Omega_{CL} = \{1, 2\}$. The global desired trajectory of leader $l \in \mathcal{V}_L^j$, $\Omega_{CL} = \{1, 2\}$ is assigned using Eq. (34), where $\beta(t)$ is specified by Eqs. (45) and (46).

The x and y components of UAV positions in the $x - y$ plane are shown in Fig. 8. It is seen that UAVs all reach their target destinations while no two UAVs collide. Fig. 9 shows deviations of all UAVs from the global desired coordination references in clusters 1 and 2. As shown the deviations of UAVs in cluster 1 are less than $\delta^1 = 0.2472m$. Also, UAV deviations in cluster 2 are less than $\delta^2 = 0.1198m$.

7.2. Case-study 2: limited airspace with no-flying zone

Clusters must avoid flying over No-Flight Zones O_1 and O_2. O_1 is a rectangular shape with vertices placed at $\mathbf{o}_1^1 = 20\hat{\mathbf{e}}_1 + 80\hat{\mathbf{e}}_2$, $\mathbf{o}_2^1 = 35\hat{\mathbf{e}}_1 + 80\hat{\mathbf{e}}_2$, $\mathbf{o}_3^1 = 20\hat{\mathbf{e}}_1 + 100\hat{\mathbf{e}}_2$, and $\mathbf{o}_4^1 = 35\hat{\mathbf{e}}_1 + 100\hat{\mathbf{e}}_2$. No Flight Zone O_2 is a triangle with vertices placed at $\mathbf{o}_1^2 =$

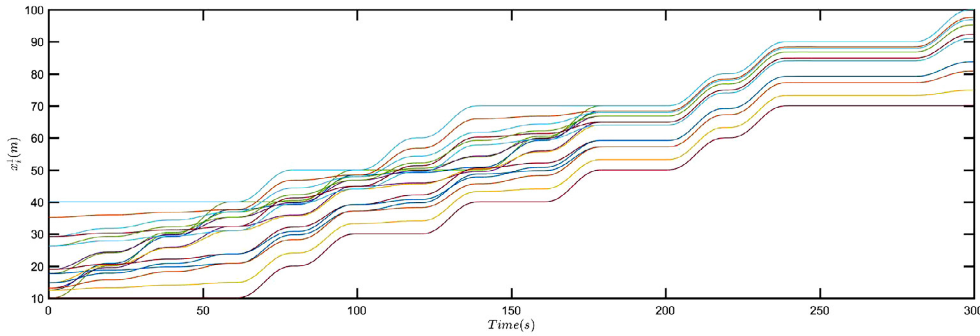

(a) x components of cluster 1

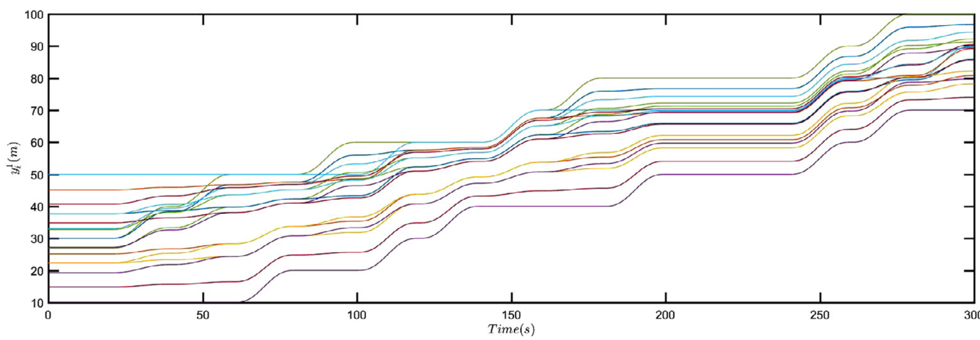

(b) y components of cluster 1

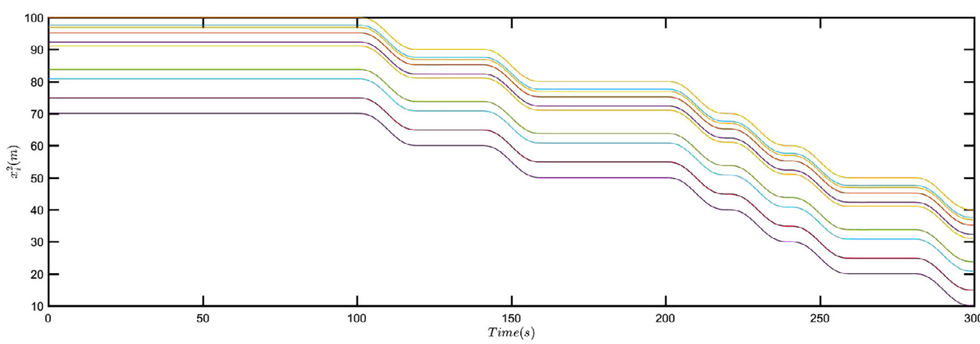

(c) x components of cluster 2

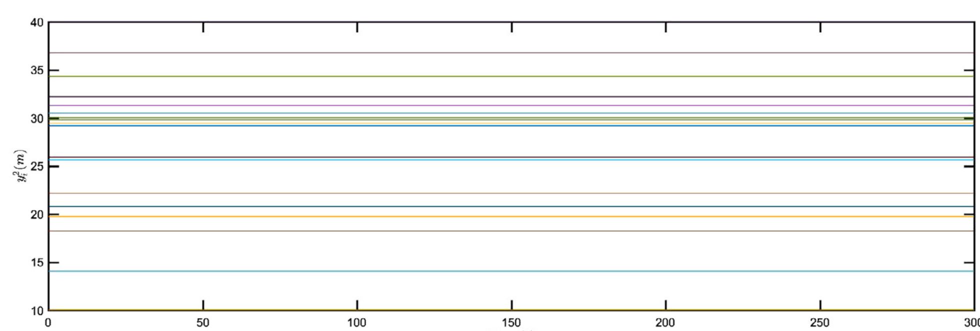

(d) y components of cluster 2

Fig. 12. Case-study 2: (a) x components of UAVs in cluster 1 versus time. (b) y components of UAVs in cluster 1 versus time. (c) x components of UAVs in cluster 2 versus time. (d) y components of UAVs in cluster 2 versus time.

$90\hat{\mathbf{e}}_1 + 50\hat{\mathbf{e}}_2$, $\mathbf{o}_2^2 = 100\hat{\mathbf{e}}_1 + 60\hat{\mathbf{e}}_2$, and $\mathbf{o}_3^2 = 85\hat{\mathbf{e}}_1 + 60\hat{\mathbf{e}}_2$. Target destinations of cluster 1 leaders are the same as in Case Study 1 but target destinations of cluster 2 leaders are different and given by: $\mathbf{r}_{1,F}^1 = 100\hat{\mathbf{e}}_1 + 70\hat{\mathbf{e}}_2 + 10\hat{\mathbf{e}}_3$, $\mathbf{r}_{2,F}^1 = 100\hat{\mathbf{e}}_1 + 100\hat{\mathbf{e}}_2 + 10\hat{\mathbf{e}}_3$, $\mathbf{r}_{3,F}^1 = 70\hat{\mathbf{e}}_1 + 90\hat{\mathbf{e}}_2 + 10\hat{\mathbf{e}}_3$, $\mathbf{r}_{1,F}^2 = 40\hat{\mathbf{e}}_1 + 10\hat{\mathbf{e}}_2 + 10\hat{\mathbf{e}}_3$, $\mathbf{r}_{2,F}^2 = 40\hat{\mathbf{e}}_1 + 40\hat{\mathbf{e}}_2 + 10\hat{\mathbf{e}}_3$, and $\mathbf{r}_{3,F}^2 = 10\hat{\mathbf{e}}_1 + 30\hat{\mathbf{e}}_2 + 10\hat{\mathbf{e}}_3$. In Figs. 10 (a-d), leaders' optimal paths connecting initial and target destinations are shown. Figs. 10 (e-h) show UAV clusters at $t = 60s$, $t = 120s$, $t = 180s$, and $t = 240s$. Leaders' optimal paths are also listed in Table 2. Eigenvalues of matrices $\mathbf{U}_{CD}^j$, denoted by λ_1^j and λ_2^j, are plotted versus time in Fig. 11 (The superscript $j = 1, 2$ is the cluster index number). Note that cluster 1 aggressively deforms

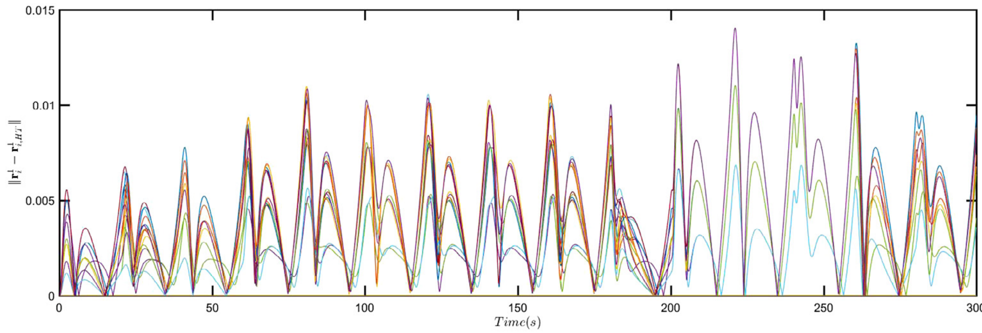

(a) Deviations of quadcopters in cluster 1

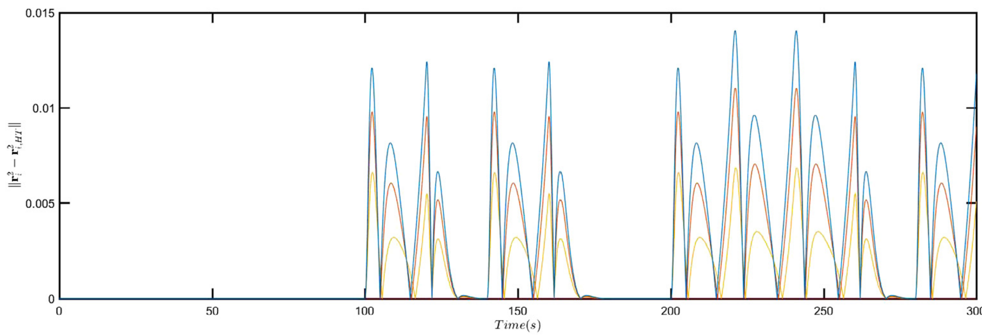

(b) Deviations of quadcopters in cluster 2

Fig. 13. Case-study 2: (a) Deviation of cluster 1 UAVs from global desired coordination. (b) Deviation of cluster 2 UAVs from global desired coordination.

in order to reach the desired final formation by passing through a narrow channel. However, cluster 2 moves as a rigid body; therefore, $\lambda_1^2(t) = \lambda_2^2(t) = 1$ at any time t. Furthermore, $\lambda_{i,j}(t) > \lambda^j_{\mathrm{CD,min}}$ at any time t ($i = 1, 2$ and $j = 1, 2$). Therefore, followers all remain inside the triangular domain defined by the cluster leaders and no two quadcopters collide while cluster 1 aggressively deforms to avoid obstacles and reach the target formation. x and y components of actual positions of quadcopters are plotted versus time in Fig. 12. Furthermore, Fig. 13 plots deviations of agents of cluster 1 and 2 from the desired continuum deformation.

8. Conclusion and future work

This paper studies the problem of multi-cluster continuum deformation optimization in which multiple UAV teams form clusters that are safely coordinated for flight through a shared motion space. By treating MUS evolution with continuum deformation for contained UAV clusters, collision-free collective motion with minimal communication and manageable planning overhead are achieved despite changes in each cluster's shape over the trajectory. The paper contributes a novel hierarchical strategy for leader planning above continuum deformation collision-free coordination. Future work is necessary to extend the triangular clusters and constraint to constant altitude to a full three-dimensional cluster shape and trajectory space.

This work is based on the assumption that the total number of agents is fixed within every cluster in a continuum deformation coordination. In future work, we aim to enhance the resilience and scalability by forming a hybrid multi-cluster deformation coordination framework with two modes: (i) "Merge-Split" and (ii) "Continuum Deformation". In the "Merge-Split" mode, our recently-proposed deployment method [52] is used to safely merge and split clusters, and reduce or increase the number of clusters. In the "Continuum Deformation" mode, the multi-cluster continuum deformation coordination approach, proposed in this paper, can be applied to safely manage coordination of many agents in an obstacle-laden environment.

Declaration of Competing Interest

None declared.

Acknowledgements

This work is dedicated to the late Professor Suhada Jayasuriya. This work has been supported by the National Science Foundation under Award Nos. 1134669, 1250280, and 1739525.

References

[1] C.G. Rieger, K.L. Moore, T.L. Baldwin, Resilient control systems: a multi-agent dynamic systems perspective, in: 2013 IEEE International Conference on Electro/Information Technology, EIT, IEEE, 2013, pp. 1–16.
[2] P. Zhao, S. Suryanarayanan, M.G. Simoes, An energy management system for building structures using a multi-agent decision-making control methodology, IEEE Trans. Ind. Appl. 49 (1) (2013) 322–330.
[3] C.H. Botts, J.C. Spall, A.J. Newman, Multi-agent surveillance and tracking using cyclic stochastic gradient, in: 2016 American Control Conference, ACC, IEEE, 2016, pp. 270–275.
[4] F. Zhu, H.A. Aziz, X. Qian, S.V. Ukkusuri, A junction-tree based learning algorithm to optimize network wide traffic control: a coordinated multi-agent framework, Transp. Res., Part C, Emerg. Technol. 58 (2015) 487–501.
[5] K.-K. Oh, M.-C. Park, H.-S. Ahn, A survey of multi-agent formation control, Automatica 53 (2015) 424–440.
[6] D. Lee, S. Kim, J. Suk, Formation flight of unmanned aerial vehicles using track guidance, Aerosp. Sci. Technol. 76 (2018) 412–420.
[7] R.T. Thien, Y. Kim, Decentralized formation flight via PID and integral sliding mode control, Aerosp. Sci. Technol. 81 (2018) 322–332.
[8] Y. Feng, K.L. Head, S. Khoshmagham, M. Zamanipour, A real-time adaptive signal control in a connected vehicle environment, Transp. Res., Part C, Emerg. Technol. 55 (2015) 460–473.
[9] B. Shirani, M. Najafi, I. Izadi, Cooperative load transportation using multiple UAVs, Aerosp. Sci. Technol. 84 (2019) 158–169.
[10] H. Rastgoftar, E.M. Atkins, Cooperative aerial lift and manipulation (calm), Aerosp. Sci. Technol. 82 (2018) 105–118.

[11] C.B. Low, Q. San Ng, A flexible virtual structure formation keeping control for fixed-wing UAVs, in: 2011 9th IEEE International Conference on Control and Automation, ICCA, IEEE, 2011, pp. 621–626.
[12] N.H. Li, H.H. Liu, Formation UAV flight control using virtual structure and motion synchronization, in: 2008 American Control Conference, IEEE, 2008, pp. 1782–1787.
[13] A. Essghaier, L. Beji, M.A. El Kamel, A. Abichou, J. Lerbet, Co-leaders and a flexible virtual structure based formation motion control, Int. J. Veh. Auton. Syst. 9 (1–2) (2011) 108–125.
[14] W. Ren, Distributed leaderless consensus algorithms for networked Euler–Lagrange systems, Int. J. Control 82 (11) (2009) 2137–2149.
[15] W. Ren, R.W. Beard, E.M. Atkins, Information consensus in multivehicle cooperative control, IEEE Control Syst. 27 (2) (2007) 71–82.
[16] L. Ding, Q.-L. Han, G. Guo, Network-based leader-following consensus for distributed multi-agent systems, Automatica 49 (7) (2013) 2281–2286.
[17] Z. Li, Z. Duan, W. Ren, G. Feng, Containment control of linear multi-agent systems with multiple leaders of bounded inputs using distributed continuous controllers, Int. J. Robust Nonlinear Control 25 (13) (2015) 2101–2121.
[18] M. Ji, G. Ferrari-Trecate, M. Egerstedt, A. Buffa, Containment control in mobile networks, IEEE Trans. Autom. Control 53 (8) (2008) 1972–1975.
[19] H. Rastgoftar, Continuum Deformation of Multi-Agent Systems, Springer, 2016.
[20] H. Rastgoftar, H.G. Kwatny, E.M. Atkins, Asymptotic tracking and robustness of MAS transitions under a new communication topology, IEEE Trans. Autom. Sci. Eng. 15 (1) (2018) 16–32.
[21] H. Rastgoftar, S. Jayasuriya, Evolution of multi-agent systems as continua, J. Dyn. Syst. Meas. Control 136 (4) (2014) 041014.
[22] H. Rastgoftar, E.M. Atkins, Continuum deformation of multi-agent systems under directed communication topologies, J. Dyn. Syst. Meas. Control 139 (1) (2017) 011002.
[23] H. Rastgoftar, S. Jayasuriya, Swarm motion as particles of a continuum with communication delays, J. Dyn. Syst. Meas. Control 137 (11) (2015) 111008.
[24] L. He, P. Bai, X. Liang, J. Zhang, W. Wang, Feedback formation control of UAV swarm with multiple implicit leaders, Aerosp. Sci. Technol. 72 (2018) 327–334.
[25] L. Cheng, Z.-G. Hou, M. Tan, A mean square consensus protocol for linear multi-agent systems with communication noises and fixed topologies, IEEE Trans. Autom. Control 59 (1) (2014) 261–267.
[26] H. Ma, D. Liu, D. Wang, F. Tan, C. Li, Centralized and decentralized event-triggered control for group consensus with fixed topology in continuous time, Neurocomputing 161 (2015) 267–276.
[27] F. Sun, K. Turkoglu, Nonlinear consensus strategies for multi-agent networks under switching topologies: real-time receding horizon approach, Aerosp. Sci. Technol. 87 (2019) 323–330.
[28] W. Hou, M. Fu, H. Zhang, Z. Wu, Consensus conditions for general second-order multi-agent systems with communication delay, Automatica 75 (2017) 293–298.
[29] M. Nazari, E.A. Butcher, T. Yucelen, A.K. Sanyal, Decentralized consensus control of a rigid-body spacecraft formation with communication delay, J. Guid. Control Dyn. 39 (4) (2016) 838–851.
[30] H. Gui, G. Vukovich, Distributed almost global finite-time attitude consensus of multiple spacecraft without velocity measurements, Aerosp. Sci. Technol. 75 (2018) 284–296.
[31] L. Wang, F. Xiao, Finite-time consensus problems for networks of dynamic agents, arXiv preprint, arXiv:math/0701724.
[32] Y. Cao, W. Ren, M. Egerstedt, Distributed containment control with multiple stationary or dynamic leaders in fixed and switching directed networks, Automatica 48 (8) (2012) 1586–1597.
[33] Y. Cao, W. Ren, Containment control with multiple stationary or dynamic leaders under a directed interaction graph, in: Proceedings of the 48th IEEE Conference on Decision and Control, 2009 Held Jointly with the 2009 28th Chinese Control Conference, CDC/CCC 2009, IEEE, 2009, pp. 3014–3019.
[34] Z. Li, W. Ren, X. Liu, M. Fu, Distributed containment control of multi-agent systems with general linear dynamics in the presence of multiple leaders, Int. J. Robust Nonlinear Control 23 (5) (2013) 534–547.
[35] Z. Meng, W. Ren, Z. You, Distributed finite-time attitude containment control for multiple rigid bodies, Automatica 46 (12) (2010) 2092–2099.
[36] Y. Zheng, L. Wang, Containment control of heterogeneous multi-agent systems, Int. J. Control 87 (1) (2014) 1–8.
[37] M. Lal, D. Maithripala, S. Jayasuriya, A continuum approach to global motion planning for networked agents under limited communication, in: 2006 International Conference on Information and Automation, ICIA 2006, IEEE, 2006, pp. 337–342.
[38] M. Lal, S. Sethuraman, S. Jayasuriya, J.M. Rojas, A new method of motion coordination of a group of mobile agents, in: ASME 2006 International Mechanical Engineering Congress and Exposition, American Society of Mechanical Engineers, 2006, pp. 1273–1279.
[39] M. Roozegar, M. Mahjoob, M. Jahromi, Optimal motion planning and control of a nonholonomic spherical robot using dynamic programming approach: simulation and experimental results, Mechatronics 39 (2016) 174–184.
[40] A. Stentz, Optimal and efficient path planning for partially-known environments, in: Proceedings of the 1994 IEEE International Conference on Robotics and Automation, IEEE, 1994, pp. 3310–3317.
[41] N.A. Melchior, R. Simmons, Particle RRT for path planning with uncertainty, in: 2007 IEEE International Conference on Robotics and Automation, IEEE, 2007, pp. 1617–1624.
[42] E.F. Camacho, C.B. Alba, Model Predictive Control, Springer Science & Business Media, 2013.
[43] X. Wang, V. Yadav, S. Balakrishnan, Cooperative UAV formation flying with obstacle/collision avoidance, IEEE Trans. Control Syst. Technol. 15 (4) (2007) 672–679.
[44] Z. Wang, S. Zlatanova, Multi-agent based path planning for first responders among moving obstacles, Comput. Environ. Urban Syst. 56 (2016) 48–58.
[45] J. Berger, N. Lo, An innovative multi-agent search-and-rescue path planning approach, Comput. Oper. Res. 53 (2015) 24–31.
[46] H. Ma, T.S. Kumar, S. Koenig, Multi-agent path finding with delay probabilities, in: AAAI, 2017, pp. 3605–3612.
[47] V.R. Desaraju, J.P. How, Decentralized path planning for multi-agent teams with complex constraints, Auton. Robots 32 (4) (2012) 385–403.
[48] V.R. Desaraju, J.P. How, Decentralized path planning for multi-agent teams in complex environments using rapidly-exploring random trees, in: 2011 IEEE International Conference on Robotics and Automation, ICRA, IEEE, 2011, pp. 4956–4961.
[49] J. Wang, C. Jiang, Z. Han, Y. Ren, R.G. Maunder, L. Hanzo, Taking drones to the next level: cooperative distributed unmanned-aerial-vehicular networks for small and mini drones, IEEE Veh. Technol. Mag. 12 (3) (2017) 73–82.
[50] H.V. Parunak, M. Purcell, R. O'Connell, Digital pheromones for autonomous coordination of swarming UAV's, in: 1st UAV Conference, 2002, p. 3446.
[51] W.M. Lai, D.H. Rubin, E. Krempl, D. Rubin, Introduction to Continuum Mechanics, Butterworth-Heinemann, 2009.
[52] H. Rastgoftar, E.M. Atkins, Deployment of an arbitrary distribution of a multi-agent system with finite size on a desired formation, in: ASME 2016 Dynamic Systems and Control Conference, American Society of Mechanical Engineers, 2016, V002T23A004.